

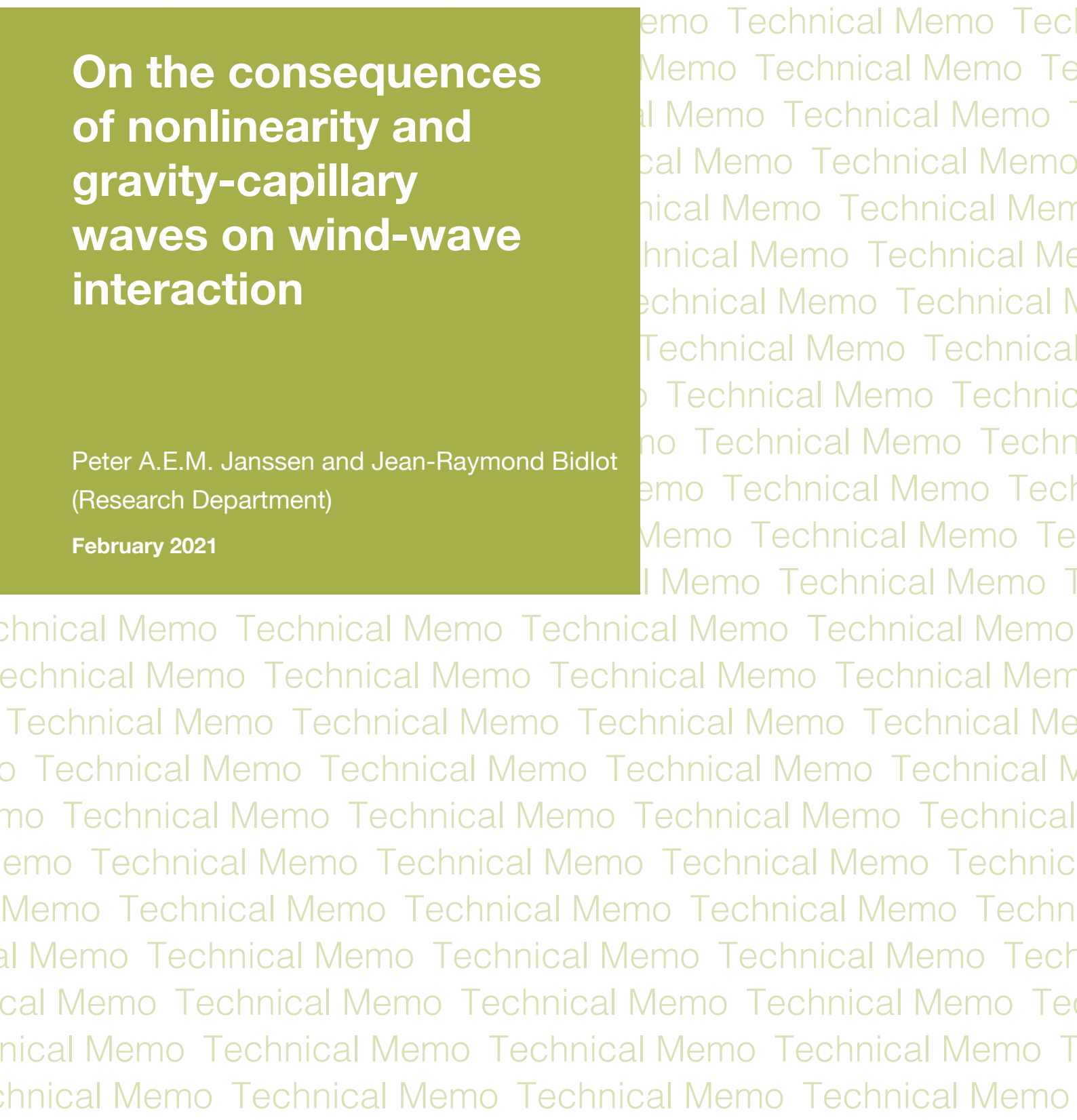
Technical Memo

882

On the consequences of nonlinearity and gravity-capillary waves on wind-wave interaction

Peter A.E.M. Janssen and Jean-Raymond Bidlot
(Research Department)

February 2021



Series: ECMWF Technical Memoranda

A full list of ECMWF Publications can be found on our website under:

<http://www.ecmwf.int/en/publications>

Contact: library@ecmwf.int

© Copyright 2021

European Centre for Medium-Range Weather Forecasts, Shinfield Park, Reading, RG2 9AX, UK

Literary and scientific copyrights belong to ECMWF and are reserved in all countries. The content of this document is available for use under a Creative Commons Attribution 4.0 International Public License. See the terms at <https://creativecommons.org/licenses/by/4.0/>.

The information within this publication is given in good faith and considered to be true, but ECMWF accepts no liability for error or omission or for loss or damage arising from its use.

Abstract

In this paper we would like to revisit the problem of the interaction of wind and waves with emphasis on strong winds. For these extreme events it is assumed that nonlinearity is so large that the slope of the wind waves has reached a limiting steepness. This limitation has been implemented in the the WAM model version at ECMWF (called ecWAM, ECMWF 2020) and has resulted in a reduced increase of the drag coefficient with wind speed in the range of large wind speed.

However, observations suggest that the drag may even decrease with increasing wind speed and here it is pointed out that in the original approach (Janssen, 1989) the assumption was made that the dimensionless background roughness gz_b/u_*^2 associated with the growth of gravity-capillary waves is a constant. Using the VIERS model an explicit calculation of the background roughness length can be made and for relatively mild winds and fairly old windsea this assumption is valid, but for young, steep windsea it is shown that the background roughness length almost vanishes. As a consequence, for strong winds having young windseas, the drag over wind waves is much reduced.

In addition, there is a strong interaction between the wind and waves. The slowing down of the wind is a nonlinear process, because it depends on the wave spectrum itself. Therefore, the growthrate of the waves by wind depends on the wave spectrum, and following work by Miles (1965) it is straightforward to obtain the sea state dependence of the growthrate. For strong winds it is found that, since the waves are typically steep, this nonlinear effect gives a further reduction of the wind input. As a consequence, in these extreme circumstances the drag coefficient may decrease with increasing wind.

1 Introduction.

In this paper we would like to present some new results on the generation of ocean waves by wind and the consequent feedback of the growing wind-waves on the airflow (called the quasi-linear effect in previous works of Janssen (1982, 1989, 1991)). In Janssen (1991) a parametrization of the effect of waves on the wind profile and the consequent slowing down was developed. This parametrization of the two-way interaction of wind and waves has been used in the operational Wam model since the end of 1991 and has produced good agreement with the most recent parametrizations of the surface drag coefficient C_D (see Edson *et al.*, 2013).¹ Nevertheless, in spite of the success of this approach, it is valid to ask a number of questions regarding some of the assumptions that have been made.

The first question concerns the stress balance. So far, in wave modelling we have only considered effects of ocean waves on the airflow in the context of an integral constraint involving stresses at the ocean surface. Denoting by $\tau_{w,lf}$ the wave-induced stress of the low-frequency gravity waves, by $\tau_{w,hf}$ the wave-induced stress of the high-frequency gravity-capillary waves and by τ_v the viscous stress, the stress balance at the surface reads

$$\tau_a = \tau_{w,lf} + \tau_{w,hf} + \tau_v \quad (1)$$

where $\tau_a = \rho_a u_*^2$ is the surface stress and u_* the friction velocity. However, it should be pointed out that the stress balance at every height above the surface should be satisfied as well. Following Miles (1965), in doing so it is found that the wind-wave growth depends on the wavenumber spectrum itself in a nonlinear manner. This is in addition to what Janssen (1991) found where the growth rate depends only in a quasi-linear manner on the wave spectrum through the surface roughness length. It turns out that steeper waves will have a smaller growthrate. This nonlinear effect is so strong that for extreme

¹ the common definition of the drag coefficient of air at a certain height $z = L$ is $C_D(L) = \tau(L)/\rho_a U(L)^2$ with $\tau(L)$ the 'surface' stress, $U(L)$ the wind speed at height L and ρ_a the air density.

winds, which typically generate steep waves, the momentum transfer from wind to waves gets reduced to such an extent that for wind speed over 30 m/s the drag coefficient reduces for increasing winds. Since the publication of Powell *et al.* (2003) showing field observations of decreasing drag coefficients in high winds, attempts have been made to explain this phenomena. Makin (2005) suggests that in high winds sea-spray droplets form a stable layer near the water surface which damps the turbulence and so reduces the drag coefficient. Others try to give a mechanical explanation for the reduction of drag for high winds. Examples are Kudryavtsev and Makin (2007) and Kukulka *et al.* (2007) who consider the sheltering of short waves due to air-flow separation. Neither can explain a decreasing drag coefficient in high winds. This also applies for the quasi-linear theory of wind-wave generation put forward by Troitskaya *et al.* (2012). Here, a fairly simple explanation of the reduction of the drag coefficient in high winds is given. It is caused by the combination of a nonlinear wind input source function and a sea-state dependent background roughness length as explained below.

The second question is related to the introduction of a background roughness length. Originally, Janssen (1989) concentrated on the effects of surface gravity waves on the mean airflow, and it was assumed that the effects of gravity-capillary waves on the airflow could be described by means of the introduction of a background roughness length z_b which is similar to the Charnock relation, but with a small value of the Charnock parameter. Thus,

$$z_b = \alpha_b u_*^2 / g, \quad (2)$$

where initially, based on a comparison with Hexos data (Janssen, 1992), it was found that $\alpha_b = 0.01$. Later work by Jean Bidlot (ECMWF, 2019) suggested a smaller value of $\alpha_b = 0.0065$.

This parametrization of the background roughness length has been used in the operational Wam model since the end of 1991 and has produced good agreement with the most recent parametrizations of the observed surface drag coefficient C_D (see Edson *et al.*, 2013). Nevertheless, in spite of the success of this approach, it is a valid question to ask why the roughness length of the gravity capillary waves would scale with the square of the friction velocity divided by acceleration of gravity g , and whether α is a constant.

Here, it is suggested to calculate the background roughness length using a model for the gravity-capillary wave spectrum called the VIERS model. This model was proposed by Janssen *et al.* (1998), and it gives the spectrum of gravity-capillary waves as follows from the balance of a nonlinear wind input source function, dissipation by wave breaking and three and four-wave nonlinear interactions. The surface stress then results from an iterative solution of the stress balance at the surface, as given in Eq. (1). An iterative solution is required because viscous stress, and the low and high frequency stress all depend in a nonlinear way on the surface stress τ_a . If the surface stress is known it is possible to obtain quantities such as the background roughness length and the drag coefficient and we will study the dependence of these quantities on wind speed U_{10} in the range $1 \leq U_{10} \leq 80$ m/s and on the wave age parameter $\chi = c_p / u_*$ where c_p is the phase speed of the peak of the wave spectrum. Regarding the validity of the background roughness length as proposed by Janssen (1991) it is found that for intermediate and older stages of development ($\chi > 15$) Eq. (2) gives order of magnitude agreement with the explicit calculation. However, there is a significant disagreement for extreme sea states being very young ($\chi < 10$). In that event the parametrisation of the background roughness (2) is seen to overestimate the roughness. In particular for hurricane cases, where young windseas are prevalent, the difference in roughness length is important, because the new formulation of the stress over the oceans (including the nonlinear form of the wind input source function) gives much smaller drag and therefore much larger wind speeds.

The programme of this paper is as follows. In §2 a brief summary of the calculation of surface stress according to Janssen (1991) is given. This work is based on critical layer theory of Miles (1957) and

the key result is that the growth rate of the waves by wind is proportional to the curvature in the mean wind profile at the critical height, while the slowing down of the wind, resulting in the drag, is found to depend on the wave spectrum. Model results for the drag are compared with the observed wind speed dependence of the drag as obtained by Edson *et al.* (2013), while its sea state dependence is validated against a parametrization found by Huang (2005). In addition, we extend the coupling approach to the case of two-dimensional wave propagation and the evolution equation for the mean flow is derived. In the steady state, and including effects of turbulence on the mean flow, one may evaluate how the curvature of the mean wind depends on the wave spectrum. Following Miles (1965), this then gives the nonlinear dependence of the growth rate of the waves by wind on the wave spectrum.

This is followed in §3 by a brief presentation of the VIERS model (Janssen *et al.*, 1998) which assumes that the gravity wave spectrum, obtained by a wave prediction system, is given while the gravity-capillary wave spectrum is obtained from the steady state version of the energy balance equation using the 'local' (in wavenumber space) approximation for the three and four-wave interactions. Using a parametrized version of Miles wind-input source function (Miles, 1957) complemented with the Quasi-linear effect of Janssen (1991) and the additional nonlinear effects found in §2, one then obtains from the gravity wave spectrum the wave-induced stress of the gravity waves $\tau_{w,lf}$ while the gravity-capillary spectrum gives the high-frequency stress $\tau_{w,hf}$. However, it is not at all guaranteed that then the stress balance at the surface, Eq. (2), is satisfied. Therefore, an iteration process is started which uses the stress balance to obtain, for given gravity wave spectrum, the total stress τ_a . Note that in every step of the iteration process one solves for the gravity-capillary spectrum, which depends on the surface stress (which varies during the iteration process) and the fixed energy flux from the gravity waves. In this fashion the stress relation at the surface can be satisfied, because it can be shown empirically that the iteration process converges.

In §4 a number of properties of the new model for surface stress are presented and the key result is a 'climatological' relation between the drag coefficient C_D and wind speed U_{10} . It is shown that up to a wind speed of about 23 m/s the drag coefficient increases with wind speed which is then followed by a maximum in drag at about 30 m/s while for higher winds a decrease of drag coefficient with wind speed is found. Below the wind speed of 23 m/s there is a good agreement with the observed wind speed dependence of the drag as obtained by Edson *et al.* (2013). The model results are also in qualitative agreement with observations of decreasing drag with wind speed for hurricane conditions. It is also shown how the wave-induced stress of the gravity waves and of the gravity-capillary waves depends on wind speed. Owing to combination of the quasi-linear effect and nonlinearity the momentum transfer to the high-frequency, gravity capillary waves is quenched for high winds when the waves are steep. As a consequence for high winds, i.e. $U_{10} > 23$ m/s, the wave-induced stress to the gravity-capillary waves $\tau_{w,hf}$ vanishes. This has important consequences for the dependence of the drag coefficient on wind speed. Also, when $\tau_{w,hf}$ vanishes it is possible to find an expression for the surface stress as according to Eq. (1), ignoring the viscous stress, the surface stress equals the low-frequency wave-induced stress. Using a simple expression for the wave spectrum and the wind input term an approximate expression for the wave-induced stress is obtained which helps explain under what circumstances C_D decreases with increasing wind speed. At around a wind speed of 30 m/s the drag coefficient attains a maximum and above that wind speed nonlinearity becomes so strong that the wind input and hence the low-frequency wave induced stress are reduced to a considerable extent. As a consequence, a reduction of the drag coefficient for increasing wind speed is found, in qualitative agreement with recent findings from observation campaigns (e.g. Powell *et al.*, 2003; Powell, 2008; Jarosz *et al.*, 2007; Holthuijsen *et al.*, 2012). Donelan (2018) tries to explain the reduction in drag in terms of flow separation which occurs just after the crest of a surface gravity wave. Flow separation is a highly nonlinear effect, that most certainly will reduce the wind input and hence will give rise to a reduced drag. In the present approach it will be seen that the nonlinear wind input plays an important role in reducing the drag.

However, one cannot be certain whether in this theoretical approach the nonlinearity solely stems from flow separation although simulations of turbulent flow over surface waves by Sullivan *et al.* (2000) do suggest the presence of flow separation when the critical layer is close to the surface. This Section is concluded with a brief discussion on the choice of a number of tuning parameters in the model. For example, results for mean square slope are compared with observations from Cox and Munk (1954) in order to determine the starting wavenumber of the model for the gravity-capillary wave spectrum.

In §5 we will discuss the work done by introducing the new model for surface stress into a private version of the ecWAM model. In order to speed up the routine for the calculations of the background roughness, an approximation to the gravity-capillary spectrum is introduced which ignores direct effects of wind input and dissipation. This so-called inertial subrange spectrum provides an accurate approximation to the wave-induced stress associated with the gravity-capillary waves. But quantities such as the mean square slope are less accurately approximated. Furthermore, because of the introduction of the effects of surface tension and viscosity, the updated ecWAM model will not obey the 'classical' scaling relations proposed already by Kitaigorodskii in 1962. In these scaling relations the relevant parameters such as wave energy, peak period, wave age, duration and fetch, etc are made dimensionless by means of acceleration of gravity g and the friction velocity u_* . For this reason the scaling is sometimes referred to as friction velocity scaling. It is found that while for young wind sea the classical scaling relations work, it will become clear that for old wind sea considerable deviations may be found.

In §6 our conclusions are summarized. The present operational version of ecWAM (Cy47R1) has an empirical cap on the Charnock parameter for strong winds (ECMWF, 2020) which we hope to replace with this new development. Also, since CY46R1, the input and dissipation source terms are based on those of Ardhuin *et al.* (2010), where the wind input source function is based on Janssen (1991) except for the partial sheltering effect. We hope to replace the sheltering effect with the new nonlinear wind input.

2 Wind-wave interaction.

Wind-wave interaction involves two aspects. First of all, waves are generated by wind, and we shall adopt for convenience a particular wind-wave generation mechanism, namely Miles' critical layer theory, which was originally formulated as a theory for the case of one-dimensional propagation. In Miles (1957) it is found that in the so-called quasi-laminar approach the critical height, which is the height where wind speed $U_0(z)$ equals the phase speed $c = \omega/k$, plays a very important role in the generation process. It turns out that the growthrate γ of the ocean waves by wind is proportional to the ratio of the curvature of the wind speed profile divided by its shear, both evaluated at the critical height. Hence, the momentum transfer from wind to waves is an example of the resonant interaction between wind and waves. The second aspect, the feedback of the growing waves on the wind, is discussed extensively by Janssen (1982, 1989, 2004). The resonant interaction process conserves momentum, hence while the waves are growing they will extract considerable amounts of momentum from the air resulting in a slowing down of the airflow. As a consequence, the drag of airflow over wind waves depends on the sea state, because young, steep wind waves will extract much more momentum from the airflow than old, gentle wind waves.

We revisit the case of two-dimensional propagation which was only partially discussed in Janssen (1991). It will be seen that the expression for the growth of ocean waves by wind is very similar to the one-dimensional result, so that the growthrate is proportional to the curvature in the wind profile. However, the mean flow equation has an additional term because the wave-induced stress $\tau_w^{(x)} = -\langle uw \rangle$ consists

of two contributions, namely one contribution giving rise to diffusion of vorticity (also present in one-dimensional theory) and a second contribution which gives rise to diffusion of momentum. In one dimension, in the absence of turbulence, the coupled system evolves towards a steady state with a linear wind profile, hence the wind-wave growth rates vanish for large times. However, in two dimensions the equilibrium wind profile is not a linear profile because the momentum diffusion contribution tries to maintain the curvature in the wind profile. As a consequence, even in the presence of air turbulence, wave growth is in two dimensions larger for waves propagating in the wind direction than in the case of one-dimensional propagation. Here, we summarize the main results while details of the calculations are given in the Appendix.

According to three-dimensional critical layer theory, waves with phase speed c propagating in the direction θ grow when the curvature in the wind, directed along the x -axis with profile $U_0(z)$, is negative at the critical height z_c . Introducing the Doppler-shifted velocity $W = U_0(z) - c/\cos\theta$ the critical height now follows from the condition $W = 0$, or $c = U_0(z_c)\cos\theta$. The growthrate of the waves by wind is essentially the same as in two dimensions. However, one needs to replace the acceleration of gravity g by $g/\cos^2\theta$ while the phase speed c is replaced by $c/\cos\theta$. Therefore, the growth of the wavenumber spectrum $F(k, \theta)$ due to wind becomes

$$\left. \frac{\partial}{\partial t} F(k, \theta) \right|_{wind} = \gamma F(k, \theta), \quad \gamma = -\varepsilon \pi c |\chi_c|^2 \frac{W_c''}{|W_c'|}, \quad (3)$$

where the growthrate γ of ocean waves by wind is proportional to the curvature $U_0'' = W''$ of the wind profile at the critical height $z = z_c$ (Miles, 1957). Here, the wave-induced velocity χ satisfies the Rayleigh equation

$$W \nabla^2 \chi - W'' \chi = 0, \quad \chi(0) = 1, \quad \chi(\infty) = 0. \quad (4)$$

A detailed discussion of the underlying physics of this problem is given in Janssen (2004).

According to Fabrikant (1976) and Janssen (1982) wave growth results in a slowing down of the airflow. For one-dimensional propagation, the ocean waves exert a wave-induced stress $\tau_w^{(x)} = -\langle uw \rangle$ on the mean flow which depends on the wave spectrum $F(k, \theta)$. This part of the wave-induced stress leads to vorticity diffusion. In the case of two-dimensional wave propagation there is an additional contribution to the x -component of the wave-induced stress which is connected to momentum diffusion. This contribution influences the mean flow but still conserves total momentum so that it is not directly connected to wave growth. Furthermore, in the 2D case there is, in principle, also a cross stress $\tau_w^{(y)} = -\langle vw \rangle$ which leads to additional turning of the wind profile. However, in the present treatment the contribution of the cross-stress will be ignored. A reason for this is that the wave-induced stress is determined to a large extent by the high-frequency waves. The response time of these short waves is small so that in practice they are in equilibrium with the wind and therefore have a symmetrical angular distribution with respect to the wind direction. Therefore, the cross stress is assumed to be small.

Let us denote the mean flow x - and y -components of the wind by U_0 and V_0 and suppose that at the present time the mean flow is in the x -direction. The mean flow equations in the absence of turbulence and viscous effects are according to the Appendix

$$\frac{\partial}{\partial t} U_0 = \frac{\partial}{\partial z} D_{\perp} \frac{\partial}{\partial z} U_0 + D_{\parallel} \frac{\partial^2}{\partial z^2} U_0 \quad (5)$$

where for gravity waves the parallel and perpendicular diffusion coefficients depend on the sea state and for surface gravity waves (hence $v_g = c/2$) these coefficients assume the simple form

$$(D_{\parallel}, D_{\perp}) = 2\pi \int_{|\theta| \leq \pi/2} d\theta \omega k^2 F(k, \theta) (\cos^2 \theta, \sin^2 \theta) |\chi|^2. \quad (6)$$

Note that in the above expressions of the diffusion coefficients there is only an integration over direction θ and not over wavenumber k . The reason for this is that the integration over wavenumber can easily be performed because the resonance condition $W = 0$ is reflected by a Dirac δ -function with argument W . As a consequence, wavenumber k and angular frequency ω are expressed in terms of the vertical coordinate z through the resonance condition $W = U_0 - c/\cos\theta = 0$ where the phase speed follows from the dispersion relation of free gravity waves. Assuming that the x -component of the wind velocity is positive and for positive c , the resonance condition implies a restriction on the values of the angle θ , i.e. $|\theta| \leq \pi/2$. This restriction reduces the θ integration domain to those waves that have a projection onto the wind direction.

The evolution equation for the y -component of the mean velocity becomes

$$\frac{\partial}{\partial t} V_0 = -\frac{\partial}{\partial z} \left(D_c \frac{\partial}{\partial z} U_0 \right) + D_c \frac{\partial^2}{\partial z^2} U_0 = -\frac{\partial}{\partial z} (D_c) \frac{\partial}{\partial z} U_0. \quad (7)$$

and remarkably the diffusion coefficients of the two processes are the same, i.e.

$$D_c = 2\pi \int_{|\theta| \leq \pi/2} d\theta \omega k^2 |\chi|^2 F(k, \theta) \sin\theta \cos\theta. \quad (8)$$

In the following it will be assumed that the wave spectrum is symmetrical with respect to the wind direction. As a consequence the cross diffusion coefficient D_c vanishes and no y -component of the mean flow is generated. Hence, Eq. (7) is ignored.

Let us now discuss the consequences of the two-dimensional version of the wind-wave coupling a bit further. Compared to the one-dimensional version given in Janssen (1982), it is seen that the first term on the right hand side of Eq. (5) is new. This term is connected to the y -component of the wave-induced velocity and is therefore connected to vortex stretching as the mean flow vortex is in the y -direction. This term will try to maintain the curvature in the wind profile and therefore it increases wave growth.

This has important consequences for the equilibrium conditions. In one dimension, in the absence of turbulence and viscosity, the mean flow would evolve towards a condition where the curvature of the wind profile vanishes (Janssen, 1982), hence wind-wave growth vanishes for large times. This is clearly not the case for the two-dimensional problem as now the rate of change of the wind velocity is proportional to a linear combination of the shear and the curvature of the wind profile, therefore wind-wave growth does not necessarily vanish for large times.

Now, the growth rate of the waves by wind is still proportional to the curvature of the wind profile. And therefore, the second term on the right-hand side of Eq. (5) is expected to be directly related to the process of the momentum transfer from wind to waves. This is indeed the case as the vertical integral from $z = 0$ to $z = \infty$ of the first term vanishes because the diffusion coefficient D_{\perp} vanishes at the boundaries, therefore the first term conserves momentum. However, the vertical integral of the second term is finite and gives the total rate of change of air flow momentum. Finally, although the first term does not affect the momentum budget it still is important because it may locally affect the curvature of the mean flow and hence the growthrate of a particular wave.

From this discussion it is seen that in the absence of turbulence and viscosity we have the following momentum conservation law in the x -direction

$$\frac{d}{dt} \left[\rho_a \int dz U_0 + \rho_w \int d\mathbf{k} P_x \right] = 0. \quad (9)$$

therefore the reduction in air flow momentum is accompanied by an increase in the x -component of the

wave momentum P_x . Similarly, one finds for the y -momentum the conservation law

$$\frac{d}{dt} \left[\rho_a \int dz V_0 + \rho_w \int d\mathbf{k} P_y \right] = 0. \quad (10)$$

and once more it is noted that if the wave spectrum is symmetrical with respect to the wind-direction then air-flow momentum in the y -direction does not change because the y -component of the wave momentum vanishes. Here, wave momentum \mathbf{P} , is defined as

$$(P_x, P_y) = \rho_w \int d\mathbf{k} \omega(\cos \theta, \sin \theta) F(\mathbf{k})$$

and, using results from the Appendix, the wave-induced stress τ_w equals the rate of change of wave momentum due to the wind, or,

$$\tau_w = \int d\mathbf{k} \left. \frac{\partial \mathbf{P}}{\partial t} \right|_{wind} = \int d\mathbf{k} \gamma \mathbf{P} \quad (11)$$

where γ is the wind-induced growth rate given in Eq. (3). Therefore, knowing the wave momentum and knowing the growthrate of ocean waves by wind one may immediately obtain the wave-induced stress exerted on the mean air flow.

In order to proceed let us now add diffusion by turbulence and molecular viscosity and let us make the steady state assumption because momentum diffusion by waves and turbulence is usually more rapid than the timescale of the growth of waves by wind. Also, because of the assumption that the wave spectrum is symmetrical with respect to the wind direction we only need to consider the x -momentum balance. In the steady state the x -momentum balance becomes

$$\frac{\partial}{\partial z} D_{\perp} \frac{\partial}{\partial z} U_0 + (v_a + D_{\parallel}) \frac{\partial^2}{\partial z^2} U_0 + \frac{1}{\rho_a} \frac{\partial}{\partial z} \tau_{turb} = 0 \quad (12)$$

where v_a is the kinematic viscosity in air and the turbulent stress is modelled by means of a mixing length model, i.e.

$$\tau_{turb} = \rho_a l^2 \left| \frac{\partial}{\partial z} U_0 \right| \frac{\partial}{\partial z} U_0, \quad l(z) = \kappa(z + z_b).$$

while κ is the von Kármán constant and z_b is a background roughness length which represents the slowing down of the airflow by additional effects such as the growth of gravity capillary waves. This process will be discussed in more detail in the next Section.

Now integrating the momentum balance over the air column from surface to infinity one finds for the total stress $\tau_a = \rho_a u_*^2$ (with u_* the friction velocity),

$$\tau_a = \tau_v + \tau_{turb} + \tau_w, \quad (13)$$

where $\tau_v = \rho_a v_a \partial U_0 / \partial z$ and the wave-induced stress τ_w is given in Eq. (11). The above relation will play a key role in subsequent developments of the coupling between wind and waves.

The interaction of wind and waves is now described by the set of Eqns. (3)-(4), (6), (11), and (12) while the surface stress is given by Eq. (13). It is remarked that the above set of equations shows that there is a strong interaction between the wind and waves. While the waves grow they extract considerable amounts of momentum from the airflow resulting in a slowing down of the wind as the windprofile is forced by the waves towards a linear wind profile. This change in windprofile, which mainly occurs close to the

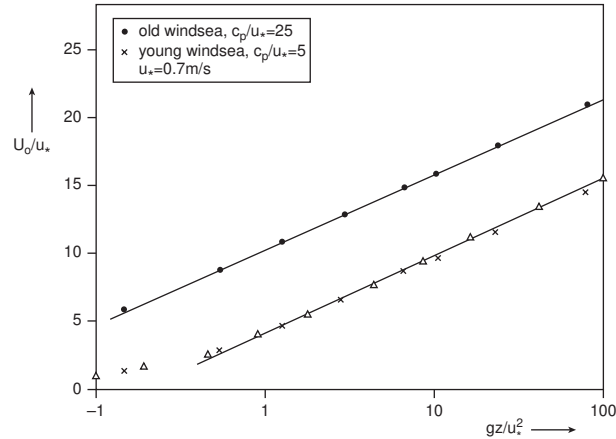


Figure 1: Effect of waves on wind profile for old and young windsea, shown by plotting dimensionless wind speed U_0/u_* as a function of dimensionless height $z_* = gz/u_*^2$. The wind profile parametrization $1/\kappa \log(1 + z_*/z_0^*)$ is denoted by a Δ . From Janssen (1989).

water surface, corresponds to an increase in roughness length and a reduction in high-frequency part of the wind input and hence the wave-induced stress.

The strong interaction of wind and waves was studied by Janssen (1989) for the one-dimensional version of the above quasi-linear set of equations (i.e. for vanishing D_\perp). The properties of the one-dimensional coupling were explored by searching for given spectral shape for steady state solutions of the airflow over wind waves by means of an iteration method. The rate of convergence of this procedure was judged by using Eq. (13), i.e. by checking how close the total stress $\tau_v + \tau_{turb} + \tau_w$ was to the surface stress $\tau_a = \rho_a u_*^2$. Typically, accuracy of 4 digits was achieved.

For the actual calculations, reported in Janssen (1989), the wave spectrum is given by the JONSWAP spectrum (Hasselmann *et al.*, 1973) with a Phillips parameter α_p which depends in a sensitive manner on the wave age $\chi = c_p/u_*$, i.e.

$$\alpha_p = 0.57\chi^{-3/2}, \tag{14}$$

hence young wind waves ($\chi = 5$) are steep while, on the other hand, old wind waves ($\chi = 25$) are gentle, corresponding to a smooth sea state.

The results of the iteration process are given in the Figs. 1 and 2. In the present context the most important result is given in Fig. 1. It shows the impact of the sea state on the wind profile. Young waves have a large roughness giving a considerable slowing down of the wind and therefore the equilibrium wind is quite reduced compared to the case of old windsea for which the airflow is much smoother. However, the shape of the wind profile away from the surface is still logarithmic, but close to the surface there are deviations from the logarithmic wind profile, which are a reflection of the impact of growing waves on the wind. In particular, it was shown in Janssen (1989) that for young windsea, the wave-induced stress dominates the total stress near the surface, giving an additional slowing down of the wind, hence a rougher airflow. Finally, Fig. 2 nicely summarizes the effect of growing waves on the wind by showing the dependence of the drag coefficient, defined as $C_D = u_*^2/U_{10}^2$, on wave age, which is in qualitative agreement with observations by Donelan (1982) and Smith *et al.* (1992). Note that the Figure also shows that results for the drag depend in a sensitive manner on how the Phillips parameter depends on the sea state. If the Phillips parameter α_p has a much less sensitive dependence on the wave age, e.g. $\alpha_p \sim \chi^{-2/3}$, the drag is virtually independent of the sea state.

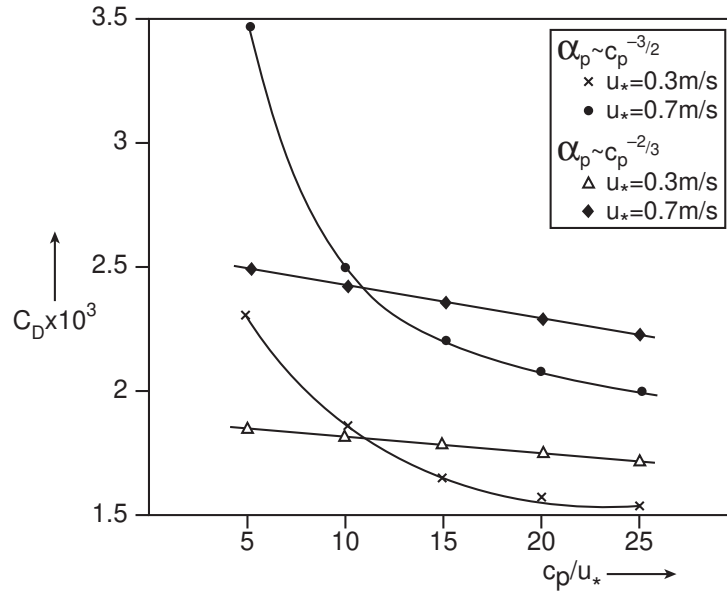


Figure 2: The wave age dependence of the drag coefficient for two different friction velocities. From Janssen (1989).

2.1 Parametrization of quasi-linear theory.

The numerical results suggest that air viscosity is not important so for the parametrization we replace Eq. (13) with the stress relation $\tau_{urb} + \tau_w = \tau_a$, or explicitly, with $l = \kappa(z + z_b)$ ²

$$z = 0: l^2 \left| \frac{\partial U_0}{\partial z} \right| \frac{\partial U_0}{\partial z} + \tau_w(z) = \tau_a, \quad (15)$$

noting that for one dimensional propagation this relation holds for every z , but in two-dimensions it only holds for $z = 0$ so we will only use the stress balance relation at the surface. In the next step we use the fit of the wind-profile to the numerical data of Janssen (1989), which is displayed in Fig. 1,

$$U_0(z) = \frac{u_*}{\kappa} \log \left(1 + \frac{z}{z_0} \right), \quad (16)$$

and substitution of the wind profile in Eq. (15) then immediately determines the roughness length z_0

$$z_0 = \frac{z_b}{\sqrt{1 - \tau_w(0)/\tau_a}} \rightarrow \alpha = \frac{gz_0}{u_*^2}. \quad (17)$$

with α the Charnock parameter. Here, $\tau_w(0)$ at the surface is obtained from the wave model.

Another advantage of using the logarithmic wind profile is that it provides a simple parameterization of the wave growth by wind. In order to obtain the growthrate γ one needs to solve the Rayleigh equation which cannot be solved exactly. In stead we use as a starting point an approximate expression for the growth rate that has been obtained by Miles (1993) by means of asymptotic matching, a result which also holds for two-dimensional propagation (see the Appendix).

²In the original treatment of Janssen (1991) $l = \kappa z$ and the boundary condition of vanishing wind speed, $U_0(z = z_b) = 0$, was specified at $z = z_b$.

With θ the wave propagation direction and ϕ the wind direction the main result for the growth rate in two spatial dimensions is

$$\gamma/\omega_0 = \varepsilon\beta \frac{u_*^2}{c^2} \cos^2(\theta - \phi), \quad (18)$$

where the Miles' parameter β is given by

$$\beta = \frac{\pi}{\kappa^2} y_c \log^4\left(\frac{y_c}{\lambda}\right), y_c \leq \lambda = \frac{1}{2} e^{-\gamma_E} = 0.281, \quad (19)$$

with $\gamma_E = 0.5771$ Euler's constant. Here, $y_c = k(z_0 + z_c)$ is the dimensionless critical height and ε is the air-water density ratio. This expression is valid for slow waves only so in order to have a reasonable approximation also for the long waves, parameters were rescaled by replacing $\lambda = 0.281$ by $\lambda = 1$, and by replacing π by the factor 1.2. In addition, in the formula for the critical height, the parameter u_*/c was shifted by the factor $z_\alpha = 0.08$. As a result the following parametrization for the Miles' parameter β is used:

$$\beta = \frac{\beta_{max}}{\kappa^2} y_c \log^4(y_c), y_c \leq 1, \quad (20)$$

with $\beta_{max} = 1.2$ and

$$y_c = kz_0 e^{\kappa/x}, x = (u_*/c + z_\alpha) \cos(\theta - \phi), z_\alpha = 0.08. \quad (21)$$

It is important to note that the above parametrization of wave growth includes the quasi-linear effect. For young waves the roughness length z_0 will be large resulting in large dimensionless critical height y_c , easily reaching values $y_c = 1$ for the short waves with large wavenumber k . In other words, the Miles parameter β , and therefore the growth rate γ , will vanish for these short waves, giving a finite wave-induced stress.

In Janssen (2004) the parametrized wave growth has been compared with observations collected by Plant (1982). Although there is a big scatter in the observations, the agreement of the parametrization with observations seems fair.

2.2 Validation of the original approach.

An extensive validation of the drag coefficient C_D of the coupled ocean-wave, atmosphere system (IFS-ecWAM, with the feedback of the waves on the airflow switched on) has been performed. Two examples are shown in Fig. 3. In the left panel the modelled sea state dependent drag at a height of half the peak wavelength is compared to a parametrization proposed by Huang (2005), which is based on observations from a number of field campaigns. It is of the form

$$C_D(\lambda_p/2) = A\chi^a, \quad (22)$$

where λ_p is the peak wavelength and the wave age χ is defined as $\chi = c_p/u_*$ with c_p the phase speed of the peak of the spectrum. The constants A and a are given by $A = 1.220 \times 10^{-2}$, and $a = -0.704$. The model relation is obtained from one global forecast by averaging $C_D(\lambda_p/2)$ as function of the wave age parameter. For large wave ages a good agreement between model and observed drag coefficient is obtained while for young windseas there is some underestimation and there is more scatter. In the right panel of Fig. 3 the drag coefficient at 10 m height as function of wind speed U_{10} is validated. The model

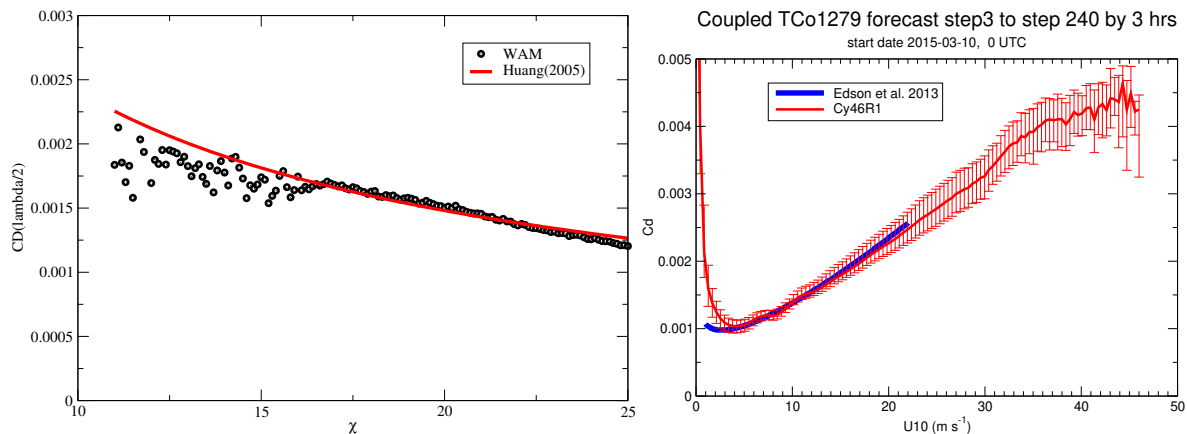


Figure 3: Left panel compares modelled drag with Huang’s (2005) empirical relation of sea-state dependent drag coefficient. The right panel compares modelled and observed (Edson *et al.*, 2013) drag coefficient relation with wind speed.

data are obtained by averaging 80 forecasts of the drag coefficient as function of wind speed. The model data are based on the version of Arhuin *et al.* (2010). The empirical fit of Edson *et al.* (2013) is obtained from eddy correlation data for the COARE 4.0 parametrization of the drag. Noting that this empirical fit is valid up to a wind speed of about 23 m/s, it is seen that on average there is a good agreement between modelled drag and observed drag. For extreme, hurricane wind speeds modelled drag shows a tendency to become less sensitive to increases in wind speed, and even shows signs of saturation. This is in qualitative agreement with empirical findings, although it must be emphasized that the scatter in the field observations is large.

As already mentioned in the introduction, an important assumption in the present approach is that the effect of the short gravity-capillary waves is represented by a background roughness length as given by Eq. (2). The validity of this assumption needs to be tested and for this reason one needs to give an explicit calculation of the momentum transfer to the short gravity capillary waves. An attempt to explicitly calculate the momentum transfer to the short waves is given in the next section, using a model for the short gravity-capillary waves, called the VIERS model (Janssen *et al.*, 1998). Before we do this we have to discuss the inclusion of nonlinear effects in the expression of the growthrate of waves by wind.

2.3 Full Nonlinear Theory.

In the previous section it has been shown that the original approach results in drag coefficients that are in good agreement with well-known parametrisations of drag against wind speed or wave age that are obtained from observation campaigns. These observational fits are restricted to wind speeds U_{10} that are less than about 23 m/s. Despite this good agreement one may question a number of assumptions underlying the original approach. Here, we discuss the validity of the assumption that the wind profile has a logarithmic shape.

The coupled equations, in particular the stress balance equation (12), show that there is a strong interaction between wind and waves. Growing waves extract considerable amounts of momentum from the airflow resulting in a slowing down of the wind. Clearly, the slowing down of the wind is a nonlinear effect, because its impact depends on the angular average of the wave spectrum. Therefore, one would expect that the growthrate of the waves by wind depends on the wave spectrum as well, and as

a consequence there would be deviations from the logarithmic wind profile. Here, a brief, approximate derivation of the sea state dependence on the growthrate is given. A similar result was already obtained by Miles in 1965, and it has been utilized in the Viers model (Janssen *et al.*, 1998, see also Caudal, 2002). This simple proof is possible because of the nature of the resonant wave, mean-flow interaction which allows a direct correspondence between wavenumber space and the vertical.

In order to start the derivation of the effect of nonlinearity it is pointed out that the growthrate of the waves by wind is according to Eq. (3) proportional to the ratio of curvature to shear of the wind profile at the critical height z_c . For a logarithmic wind profile this ratio is given by $W_c''/W_c' = -1/z_c$ for large z_c and it is of interest to learn to what extent nonlinearity will affect the curvature shear ratio. Now, from the stress balance Eq. (12) one finds for this ratio at the critical height z_c

$$\frac{W_c''}{W_c'} = - (D'_\perp + 2l_c l'_c U'_0) / (v_a + D_W + 2l_c^2 U'_0) \quad (23)$$

and because the curvature shear ratio is evaluated at the critical height this a relation in wavenumber space. Here, $D_W = D_\perp + D_\parallel$ and a prime denotes differentiation with respect to z_c . For a linear system with a logarithmic wind profile one would ignore the wave diffusion coefficients and the curvature-shear ratio would, as expected, reduce to $W_c''/W_c' = -l'_c/l_c = -1/z_c$ for large z_c .

Eliminating the ratio of curvature to shear in the expression for the growthrate in Eq. (3) one finds

$$\gamma = \varepsilon \pi c |\chi_c|^2 (D'_\perp + 2l_c l'_c U'_0) / (v_a + D_W + 2l_c^2 U'_0) \quad (24)$$

Now, define the growthrate γ_0 according to linear theory as the growthrate at $D_W = D_\perp = 0$, i.e.

$$\gamma_0 = \gamma(D=0) = \varepsilon \pi c |\chi_c|^2 l'_c/l_c / (1 + \tilde{v}_a), \quad (25)$$

with $\tilde{v}_a = v_a/2l_c^2 U'_0$. The above expression allows one to write $|\chi_c|^2$ in terms of the growthrate according to linear theory, i.e.

$$|\chi_c|^2 = \gamma_0 (1 + \tilde{v}_a) / \varepsilon \pi c l'_c/l_c \quad (26)$$

Using the expression for $|\chi_c|^2$ one can evaluate the wave diffusion coefficients. For example,

$$D_W = 2\pi \int d\theta \omega k^2 F(k, \theta) |\chi_c|^2 = \frac{2k^3}{\varepsilon l'_c/l_c} (1 + \tilde{v}_a) \int d\theta \gamma_0 F(k, \theta). \quad (27)$$

Similarly, for D_\perp one finds

$$D_\perp = \frac{2k^3}{\varepsilon l'_c/l_c} (1 + \tilde{v}_a) \int d\theta \gamma_0 F(k, \theta) \sin^2 \theta. \quad (28)$$

Hence, apart for the \sin^2 factor the expressions for the wave diffusion coefficients are identical.

in the next step, in order to evaluate the growthrate γ we need to evaluate the factor D'_\perp hence we need the height dependence of the perpendicular wave diffusion coefficient. Recall the mapping between wavenumber space and vertical space through the resonance condition $W(z_c) = 0$ which implies the simple relation $c = U_0(z_c) \cos \theta$. Here, in first order of approximation the wind profile assumes the logarithmic profile with roughness length z_0 , as given by Eq. (16). Therefore each wave related factor in the expression for D_\perp involves a logarithmic function of height. Now, evaluating D_\perp using the mixing length $l(z) = \kappa(z + z_b)$ one finds for large z

$$D_\perp = \frac{2k^3 z_c}{\varepsilon} (1 + \tilde{v}_a) \int d\theta \gamma_0 F(k, \theta) \sin^2 \theta. \quad (29)$$

The wavenumber dependent parts of the growthrate γ_0 and the wave spectrum can all be expressed in terms of the phase speed hence through the resonance condition they contain a logarithmic dependence on z_c which is slowly varying compared to a linear dependence on z_c . Only the front factor, which is linearly dependent on z_c and the $\tilde{v}_a = v_a/2\kappa z u_*$ factor which depends on the inverse of z_c are rapidly varying functions of height. To a good approximation the z_c derivative of D_\perp therefore becomes

$$D'_\perp = \frac{2k^3}{\varepsilon} \int d\theta \gamma_0 F(k, \theta) \sin^2 \theta. \quad (30)$$

Finally, using the expressions for $|\chi_c|^2$, D_W and D'_\perp in Eq. (24), one obtains for the growthrate the simple form

$$\gamma = \gamma_0 \frac{1 + N_1}{1 + N_2} \quad (31)$$

where the renormalisation factors N_1 and N_2 depend on the angular average of the product of linear growth rate and the wavenumber spectrum. They read

$$N_1 = \frac{k^3}{\varepsilon \kappa u_*} \int d\theta \gamma_0 F(k, \theta) \sin^2 \theta, \quad N_2 = \frac{k^3}{\varepsilon \kappa u_*} \int d\theta \gamma_0 F(k, \theta). \quad (32)$$

Note the similarities between the renormalisation factors, the only difference is the additional factor of $\sin^2 \theta$ in the angular average in N_1 . For typical angular dependencies in growthrates and two-dimensional spectra the difference in size between N_1 and N_2 is a factor of 6, hence $N_1 = N_2/6$. The growthrate γ_0 is the one according to linear theory with a logarithmic wind profile. For practical applications we will use the parametrization for γ_0 given in Eqns. (18), (20) and (21) with a first-guess value of the parameter β_{max} of 1.2.

In order to study the importance of the nonlinear corrections to the growthrate of the wind waves we will replace the angular average by a factor times the product of wind input in the wind direction and the wavenumber spectrum $F(k)$. For example, N_2 becomes

$$N_2 = \Delta_\gamma \frac{k^3}{\varepsilon \kappa u_*} \gamma_0(k, \theta = 0) F(k). \quad (33)$$

where the choice for the magnitude of Δ_γ is guided by the following consideration. Assume that the wave spectrum has a \cos^2 directional distribution. Hence,

$$F(k, \theta) = \frac{1}{N} \cos^2 \theta F(k), \quad N = \pi/2$$

Since the growthrate according to Eq. (18) is also proportional to $\cos^2 \theta$ the directional terms give rise to a correction factor

$$\Delta_\gamma = \frac{1}{N} \int_{-\pi/2}^{\pi/2} d\theta \cos^4 \theta = \frac{3}{4}$$

hence we take $\Delta_\gamma = 3/4$. Estimating the magnitude of N_1 involves an additional factor $\sin^2 \theta$. The relevant integral equals $1/8$ or $N_1 = N_2/6$. Since $N_1 < N_2$ nonlinear effects reduce the growthrate.

Using the approximations for N_1 and N_2 we have plotted in Fig. 4 for two wind speeds the impact of the nonlinear corrections on the growthrate as function of wavenumber k by comparing the linear normalized growthrate γ_0/ω with the nonlinear normalized growth γ/ω where γ is given by (31) and

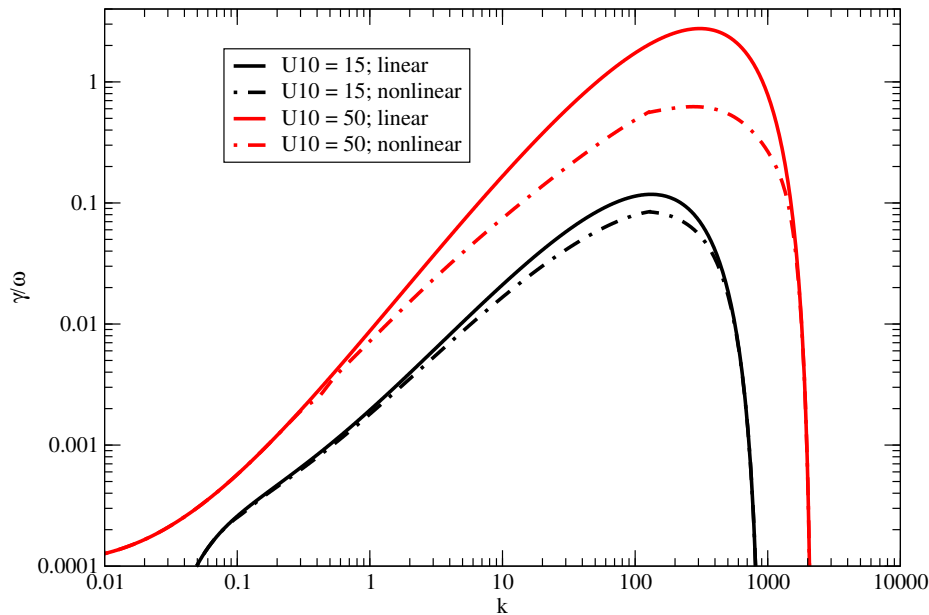


Figure 4: Dependence of linear and nonlinear growthrate on wavenumber for a low wind speed of 15 m/s and a high wind speed of 50 m/s.

the renormalisation factors N_2 is given in (33) while $N_1 = N_2/6$. The relevant solutions for the drag coefficient C_D and the friction velocity u_* are obtained using an iteration scheme as described in Section 4. From the Figure it is striking to see that nonlinear effects are only relevant for the short waves with $k > 1$. Because for critical layer theory there is a direct correspondence between height z and wave number k through the resonance condition it immediately follows that only the wind profile close to the surface deviates from the logarithmic profile due to nonlinear effects. Furthermore, the Figure also illustrates that the nonlinear effect may be quite important for strong winds of the order of 50 m/s, but it only plays a small role for 'moderate' wind speeds of the order of 10-20 m/s. This suggests that for relatively low wind speeds, the use of the logarithmic wind profile (16) is justified. Hence, the original approach seems to be valid for wind speeds less than about 20 m/s.

3 A model for the short waves.

The model for the short waves is based on work done by the VIERS-1 group in the 1990's. The main objective of this group was to obtain a physics-based model for the radar backscatter, and one of the main tasks was to obtain a model of the short gravity-capillary waves, because these short waves give an important contribution to the radar backscatter through the Bragg scatter mechanism. A detailed description of the short wave model is given in Janssen *et al.* (1998) and therefore we will suffice with a brief explanation, discussing mainly deviations from the original model, which solves the one-dimensional energy balance equation in wavenumber space. For directional aspects we refer to Caudal (2003).

The model for the short wave spectrum is based on the energy balance equation, which is solved under

steady state circumstances because the short waves have a very short response timescale. Also advection of short wave energy is disregarded, and the energy balance equation therefore reads

$$S_{in} + S_{nonl} + S_{visc} + S_{br} + S_{slicks} = 0, \quad (34)$$

where S_{in} represents the input of wind to waves, S_{nonl} describes three- and four-wave interactions, S_{visc} describes viscous dissipation, S_{br} describes dissipation due to whitecapping, and S_{slicks} describes the resonant energy transfer between surface waves and slicks (Marengoni effect). The energy balance equation is solved as a boundary value problem in wavenumber space by providing the energy flux from the long to the short waves at a boundary $k = k_{3w}$ which is basically the wavenumber where three-wave interactions start to become important.

In order to determine the energy flux at the boundary $k = k_{3w}$, knowledge of the gravity part of the wave spectrum is required. Here, in the model development phase JONSWAP spectra in wavenumber space are used while later in the paper modelled gravity wave spectra will be used. Assuming that the boundary is in the tail of the spectrum because k_{3w} is at a sufficiently high wavenumber, the spectrum $F(k)$ at the boundary is given by

$$F(k_{3w}) = \frac{1}{2} \alpha_p k_{3w}^{-4}, \quad (35)$$

so that at the boundary the spectrum is given by the Phillips' spectrum with Phillips parameter α_p which depends on wave age χ according to the scaling relation

$$\alpha_p = A \chi^{-B},$$

with $A = 0.24$ and $B = 1$. This choice of parameters is in fair agreement with the reanalysis of JONSWAP data performed by Günther (1981). Note that JONSWAP observations were obtained at fairly modest wind speed observations of the order of 10 m/s, and as a consequence the sea state was usually fairly old. The above scaling law suggests that the Phillips parameter would continue to increase for decreasing wave age χ , but since waves do have a limiting steepness it seems likely that also the Phillips parameter is limited. This saturation behaviour of the Phillips parameter has been modelled by a tanh-profile so that

$$\alpha_p = \alpha_{max} \tanh(A \chi^{-B} / \alpha_{max}), \quad \alpha_{max} = 0.031. \quad (36)$$

The appropriateness of the choice of maximum value for α has been extensively tested at ECMWF by Jean Bidlot and by Jean-Michel L  f  vre and Lotfi Aouf at M  teo France during the MyWave project. It is remarked that the choice for a limiting steepness and Phillips' parameter will have important consequences for the behaviour of the surface stress for young wind seas.

For wavenumbers higher than k_{3w} a new regime is entered because three wave interactions start to play a role in the steady state energy balance equation. In the following we shall only discuss a theory for the one-dimensional wavenumber spectrum, while, if needed, effects of the angular distribution of the short waves is provided in a fairly simple fashion.

The one-dimensional wavenumber spectrum $F(k)$, which is related to the Fourier transform of the auto-correlation of the surface elevation η , is normalized in such a way that

$$\int_0^\infty k dk F(k) = \langle \eta^2 \rangle, \quad (37)$$

where $\langle \eta^2 \rangle$ is the wave variance. The wave energy E , apart from a factor ρ_w , then follows from

$$E = \frac{\omega^2}{k} F(k), \quad (38)$$

where we shall only consider pure gravity-capillary waves with dispersion relation

$$\omega(k) = \sqrt{gk + Tk^3}, \quad (39)$$

where g is acceleration of gravity and T is surface tension.

3.1 Wind input source function.

Let us now describe some of the details of the source terms in the energy balance equation (19). For the input source function we take

$$S_{in} = \gamma F, \quad (40)$$

where γ is given by the one-dimensional version of Eq. (31). After some rearrangement one finds

$$\gamma = \gamma_0 \frac{1 + \alpha_1 \gamma_0}{1 + \alpha_2 \gamma_0} \quad (41)$$

with

$$\alpha_2 = \Delta_\gamma \frac{k^3 F(k)}{\kappa \epsilon u_*}$$

while $\alpha_1 = \alpha_2/6$. Furthermore,

$$\gamma_0 = \epsilon \beta \omega \frac{u_*^2}{c^2} \quad (42)$$

and β is given by Eqns. (20-21). The form for the growthrate is also assumed to be valid for gravity-capillary waves. We have seen that for relatively low wind speeds ($U_{10} < 20$) nonlinear effects are small so that $\gamma \approx \gamma_0$. Plant (1982) compared this expression for the growthrate γ of the waves with empirical data and he found that on average the coefficient $\epsilon \beta$ has the value of 26. However, in the context of quasilinear theory the parameter β is not a constant (see e.g. Eq. (20)) and it even vanishes when the dimensionless critical height y_c is equal to or larger than 1. This typically occurs for the short waves. The vanishing of the growthrate for short waves has, as already pointed out, an important consequence for the wave-induced stress since it remains finite for the well-known Phillips' spectrum. In order to see this recall that the wave-induced stress is basically the rate of change in time of the wave momentum due to wind, or,

$$\tau_w = \int d\mathbf{k} \gamma P \quad (43)$$

with wave momentum $P = \rho_w \omega(\mathbf{k}) F(\mathbf{k})$, while the growthrate γ is given by (41). The wave-induced stress is evaluated for the Phillips spectrum

$$F(k, \theta) = \begin{cases} \frac{1}{2} \alpha_p k^{-4}, & k > k_p \\ 0, & k < k_p \end{cases} \quad (44)$$

assuming unidirectional waves. Directionality will be taken into account separately by using a correction factor as given below. The choice of the Phillips spectrum is a reasonable guess because most of the momentum is carried by the high-frequency gravity waves, which have a k^{-4} spectral tail. In keeping with the vanishing of the growthrate at $y_c = k_c(z_0 + z_c) = 1$, a wavenumber cut-off $k = k_c$ is introduced

and the growth parameter β is assumed to be a finite constant in the range $k_p < k < k_c$ while it vanishes outside that range. Note, however, that this crude parametrization of the quasi-linear effect may affect the wave-induced stress value. For this reason we therefore have chosen an average value of β which deviates somewhat from its typical value of 26, namely $\beta = 27.5$.

Now, substitute (41) and (44) into the expression for the wave-induced stress (43) and let us restrict our attention to surface gravity waves only. Then, after some algebra we find for the wave-induced stress, normalised with the air-stress τ_a ,

$$\frac{\tau_w}{\tau_a} = \alpha_p \beta \Delta_\phi \int_{\omega_p}^{\omega_c} \frac{d\omega}{\omega} \frac{1 + \frac{1}{6} \frac{\omega}{\nu}}{1 + \frac{\omega}{\nu}} \quad (45)$$

where $\nu = 2\kappa g / \alpha_p \beta \Delta_\phi u_*$, and ω_p and ω_c are the peak and cut-off angular frequencies corresponding to the peak wavenumber k_p and the cut-off wavenumber k_c . By studying the integrand of Eq. (45) for large ω , it is clear that it is essential to have a wavenumber cut-off because otherwise there would be a logarithmic singularity for the Phillips spectrum. In other words, for gravity waves, the quasi-linear effect is essential for obtaining a finite answer for the strength of the coupling between wind and waves. This latter statement is, however, not true when capillary effects are taken into account.

Remark: Directional effects have been taken into account through the factor Δ_ϕ . Assuming that the wind blows in the x -direction, the wind input term then involves an additional factor of $\cos^2 \theta$ where θ is the propagation direction. In addition, assuming that the wave spectrum is symmetrical with respect to the wind direction, only the x -component of the wave-induced stress is finite, while, because of symmetry, the cross component vanishes. Hence, the total stress involves an additional factor $\cos \theta$. Finally, in order to get an idea about the importance of directional effects a \cos^2 directional distribution for the wave spectrum is assumed. Then, with $N = \pi/2$, the correction factor Δ_ϕ becomes

$$\Delta_\phi = \frac{1}{N} \int_{-\pi/2}^{\pi/2} d\theta \cos^5 \theta = \frac{32}{15\pi} \approx 0.68.$$

In practice, the parameter Δ_ϕ was used as a tuning parameter to ensure that for the lower wind speeds, i.e. $U_{10} < 23$ m/s, agreement with the Edson *et al* empirical fit for the drag coefficient was obtained. This resulted in an optimal value of $\Delta_\phi = 0.62$, suggesting that either wind input or wave spectrum are broader than indicated above. In fact, using the updated version of the ecWAM model, to be discussed in §5, it turns out that the optimal value of Δ_ϕ is adequate.

Performing the integration over angular frequency ω the normalised wave-induced stress assumes the simple form

$$\frac{\tau_w}{\tau_a} = \alpha_p \beta \Delta_\phi \left[\log \frac{\omega_c}{\omega_p} - \frac{5}{6} \log \frac{(\omega_c + \nu)}{(\omega_p + \nu)} \right]. \quad (46)$$

The normalised wave-induced stress measures the strength of the coupling between the wind and the surface gravity waves. According to Eq. (46) τ_w/τ_a is proportional to product of the Phillips parameter and logarithms involving the cut-off angular frequency ω_c and the angular frequency ω_p , and hence the sea state dependence of the normalised wave-induced stress is determined by how α_p and, say, the ratio ω_c/ω_p depend on the wave age χ . Typically, for increasing wave age waves become more gently, hence the Phillips parameter α_p decreases while the range parameter ω_c/ω_p increases since older wind sea implies longer waves hence a decrease in angular peak frequency. Therefore, as already discussed in Janssen (1989), the wave-age dependence of the wave-induced stress depends on the competition of these two factors. It turns out that for the presently chosen sensitive wave age dependence of α_p (see Eq. (36)) the wave-induced stress will decrease with increasing wave age. The exception is for very young wave age, $\chi < A/\alpha_{max}$, when the Phillips parameter approaches the constant value α_{max} . Under these

circumstances, the normalized wave-induced stress will increase with increasing wave age. In other words, the wave-induced stress will attain a maximum for wave ages of the order of 5-10. As will be evident in Section 4, this special behaviour of the wave-induced stress will have profound consequences for the dependence of the drag on wind speed in hurricane conditions.

Remark: In the original VIERS model a slightly different input source function was used. It had a similar form as in Eq. (41), but with α_1 vanishing because at that time it was not realized that for two-dimensional propagation there was an extra contribution to maintain the curvature in the wind profile.

3.2 Nonlinear interactions.

Following Kitaigorodskii (1983), it is assumed that the nonlinear transfer is a local process in wavenumber space, and introducing the energy flux $\Phi(k)$ one thus has

$$S_{nonl} = -\frac{1}{k} \frac{\partial}{\partial k} \Phi(k) \quad (47)$$

and on dimensional grounds the expression for $\Phi(k)$ reads

$$\Phi(k) = \frac{c^4}{v_g} [\alpha_3 B^2 + \alpha_4 B^3] \quad (48)$$

where v_g is the group velocity $\partial\omega/\partial k$, B is the angular average of the degree of saturation (Phillips, 1985),

$$B = k^4 F(k) \quad (49)$$

while α_3 and α_4 give the strength of the three- and four-wave interactions, respectively. The coefficients α_3 and α_4 may still depend on the ratio c/v_g . In particular, α_3 should vanish in the gravity wave regime because three-wave interactions are not possible there. For this reason k_{3w} is chosen in such a way that it is connected to the minimum in the phase velocity $c = \omega/k$. This minimum occurs at $k = k_0 = \sqrt{g/T}$ and therefore

$$k_{3w} = y \sqrt{\frac{g}{T}}, \quad (50)$$

where the parameter y is typically less than one. A satisfactory choice that was tried is $y = 1/2$, but a more refined choice was proposed by J. Janssen and H. Wallbrink (1997) who made improvements to the original Viers model with the aim to obtain a better agreement between observed and simulated radar backscatter σ_0 . They found a better agreement when the starting wave number was chosen to depend on the friction velocity u_* . Based on their work we have chosen for the starting wave number

$$k_{3w} = y \left(\frac{g}{T}\right)^{1/2}, \quad y = \frac{1}{1.48 + 2.05u_*} \quad (51)$$

where instead of being a constant, y now depends on the friction velocity in such a way that in agreement with the observations of Jähne and Riemer (1990) (and of Donelan and Plant (2009)) the gravity-capillary spectrum extends over a wider wavenumber range for stronger winds. The choice of the coefficient y will be further discussed in §4 when results for mean square slope are compared with observations of Cox and Munk (1954).

In the VIERS model three dissipative processes are assumed to play a role in the gravity capillary regime, namely viscous dissipation, wave breaking and damping due to slicks. These processes have been described in some detail by Janssen *et al.* (1998) and will be denoted in this paper by $S_{diss} = -\gamma_d F(k)$. In the numerical experiments discussed here effects of damping due to slicks will be ignored.

3.3 Exact solution of short-wave energy balance.

Combining now the explicit expressions for the source terms, the energy balance equation (19) becomes

$$\frac{\partial}{\partial k} \Phi(k) = \Gamma \frac{\omega^2}{k^4} B \quad (52)$$

where the parameter Γ is defined as

$$\Gamma = \varepsilon \beta \omega \left(\frac{u_*}{c} \right)^2 - \gamma_d \quad (53)$$

and hence gives the net effect of wind input and dissipation. Note that the energy flux $\Phi(k)$, as given by Eq. (48), is a function of the degree of saturation $B(k)$. Since in practice the degree of saturation B is of the order 0.1 or less, it is a fair approximation to disregard four-wave interactions in the expression for the energy flux. Retaining therefore only three wave interactions, the energy balance equation (52) may be solved exactly,³ and the result for the degree of saturation becomes

$$B = \left(\frac{v_g}{\alpha_3} \right)^{1/2} c^{-2} \left\{ \Phi_0^{1/2} + \frac{1}{2\alpha_3^{1/2}} \int_{k_{3w}}^k dk \frac{\Gamma}{k^2} v_g^{1/2} \right\} \quad (54)$$

where Φ_0 is the value of the energy flux at $k = k_{3w}$. It is of interest to discuss the terms in (54) separately. The first term is related to the effect of three-wave interactions. In the absence of wind input and dissipation it follows from the condition of a constant energy flux in wavenumber space. The resulting spectrum is called the inertial subrange spectrum. Using the dispersion relation for pure gravity-capillary waves, the degree of saturation according to the constant energy flux condition becomes

$$B_{3w} = \left(\frac{\Phi_0}{2\alpha_3} \right)^{1/2} c_0^{-3/2} \frac{y(1+3y^2)^{1/2}}{(1+y^2)(y+y^3)^{1/4}} \quad (55)$$

where $y = k/k_0$, $k_0 = (g/T)^{1/2}$ is the wavenumber that separates gravity waves and capillary waves, and $c_0 = (gT)^{1/4}$ (note that the minimum phase speed equals $c_0\sqrt{2}$). Therefore, in the gravity wave range ($k < k_0$), the degree of saturation increases with wave number like $k^{3/4}$, while in the capillary range, B_{3w} decreases with wavenumber like $k^{-3/4}$ and it attains its maximum value at $k \approx 1.32k_0$.

Effects of wind input and dissipation (Γ -term) are represented by the second term in (54) and result in a modification of the 'inertial' subrange spectrum given in (55). The degree of saturation now becomes a function of the friction velocity while, for large wavenumbers, dissipation becomes important giving a rapid decay in the high wavenumber range. Examples of degree of saturation spectra for different wave ages (ranging from a wave age χ between 5 and 25 in steps of 5) at a constant wind speed of 15 m/s are shown in Fig. 5. The kink in these spectra is at the wavenumber $k = k_{3w} = y(u_*)k_0$ where the three wave interactions are switched on, and therefore marks the start of the gravity-capillary wave spectrum. More details of the properties of these spectra are discussed in §4.

³although Eq. (54) is not an explicit expression for the degree of saturation B since the growth rate of the waves depends through the roughness length and the friction velocity on B . Strictly speaking an iteration of (54) is required.

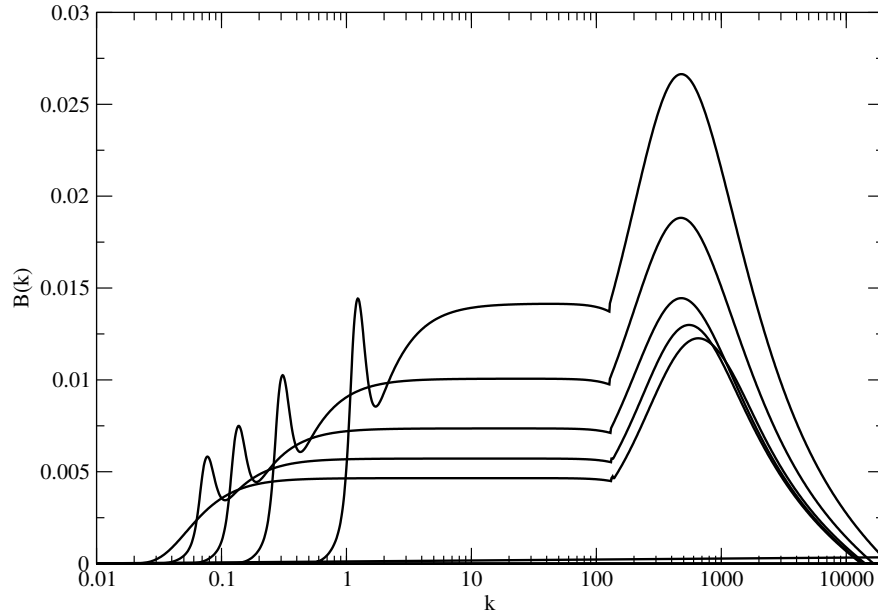


Figure 5: The wave age dependence (between 5 and 25 in steps of 5) of the degree of saturation spectrum as function of wavenumber for a wind speed of 15 m/s.

4 Determination of the surface stress.

4.1 Method.

The present model of the sea state now consists of two parts. The spectrum of the long gravity waves is provided by a wave prediction system while the spectrum of the short waves is given by the short-wave model of §3. Both models assume that the stress τ_a or the friction velocity $u_* = \sqrt{\tau_a/\rho_a}$ is given. But in practice both the long waves and, as will be seen to some extent, the short waves determine how large the momentum loss is at the interface of air and water, therefore an additional constraint is required to determine the surface stress. Assuming steady state conditions this constraint is provided by conservation of momentum at the surface. This conservation law is given in Eq. (13) and it will be repeated here:

$$\tau_a = \tau_v + \tau_{turb} + \tau_w,$$

where⁴ $\tau_v = \rho_a \bar{v}_a \partial U_0 / \partial z$, with $\bar{v}_a = v_a / 25$, and the wave-induced stress is given by

$$\tau_w = \tau_{w,lf} + \tau_{w,hf} = \int_0^\infty k dk \int_0^{2\pi} d\theta \gamma P$$

with wave momentum $P = \rho_w \omega(\mathbf{k}) F(\mathbf{k})$, while the renormalized growthrate γ is given by (31) and (33). Furthermore, the growthrate according to linear theory, γ_0 , is given by (18) and (20). Since now we have an explicit model for the background roughness, the turbulent stress, as given below Eq. (12), simplifies

⁴According to van Driest (1951) (and lab experiments) there is an interaction between turbulence and viscosity which reduces the effectiveness of the viscous stress by a factor of 25.

to

$$\tau_{turb} = \rho_a l^2 \left| \frac{\partial}{\partial z} U_0 \right| \frac{\partial}{\partial z} U_0,$$

where now the mixing length does not contain the background roughness, hence $l(z) = \kappa z$. As a consequence, the turbulent stress vanishes at the surface so that the surface stress follows from

$$\tau_a = \tau_v + \tau_{w,lf} + \tau_{w,hf}. \quad (56)$$

by iteration. In this manner a consistent solution for the spectrum of short and long-waves is obtained and at the same time a consistent estimate of the stress over growing wind waves is found.

The final part of the solution procedure concerns a method to generate realistic spectra, using the JON-SWAP spectrum. In the first step a first guess of the wave age $\chi = c_p/u_*$ is taken and a wind speed U_{10} is chosen. Using a constant drag coefficient $C_D = 1.510^{-3}$ a first guess for the friction velocity u_* is obtained and using the first guess for wave age the value of the phase speed c_p is determined. The Phillips parameter α_p then follows from Eq. (36). Hence, the spectral parameters α_p and, the peak frequency ω_p are now known so that the wave spectrum can be determined. During the iteration process the wave spectrum is kept fixed while the surface stress or friction velocity is updated every step until convergence is obtained. The convergence criterion is that the relative error in u_* is less than 10^{-5} . Convergence is always achieved but may require in the order of 100 iterations.

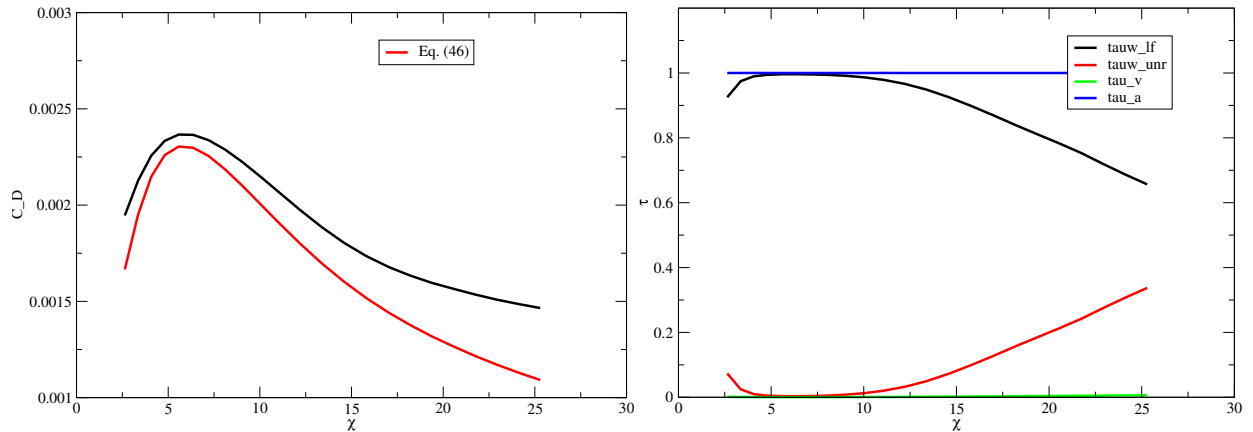


Figure 6: Left panel shows the wave age dependence of the drag coefficient for a wind speed of 15 m/s. The red line shows an approximate solution for the stress balance, Eq. (46). The right panel shows for the same wind speed the wave age dependence of the normalised low and high frequency stress.

4.2 First Results and comparison with approximate C_D .

First results of the degree of saturation spectrum for the case of a wind speed of 15 m/s and wave ages ranging from $\chi = 5$ to $\chi = 25$ are shown in Fig. 5. The short wave spectra are in qualitative agreement with the observations obtained by Jähne and Riemer (1990) (see for a later reference Donelan (2018)). For an illuminating discussion of this comparison please consult Caudal (2002).

The kink in these spectra is at wavenumber $k = k_{3w} = y(u_*)k_0$ where the three wave interactions are switched on, and therefore this marks the start of the gravity-capillary wave spectrum. Thus, rather than being constant (as for the high-wavenumber part of the gravity range), the degree of saturation increases rapidly up to about $k = 1.3k_0$, after which it rapidly decays to zero. Note that if the degree of saturation spectrum is a constant then, as pointed out in §3.1, the wave-induced stress has a logarithmic singularity, unless the quasi-linear effect is taken into account. However, for gravity-capillary waves, there is, as is clear from Fig. 5, not such a catastrophe as the degree of saturation spectrum vanishes for large wavenumber so even in the linear approximation a finite wave-induced stress results. Nevertheless, the quasi-linear effect will be seen to play a vital role in limiting the drag for high wind speeds.

In Fig. 6 the wave age dependence of the drag coefficient $C_D(z = 10)$ is shown for a wind speed of 15 m/s. The graph shows that for old windsea ($\chi \approx 25$) the drag coefficient is quite low and it increases with decreasing wave age until a maximum of 2.25×10^{-3} is reached for $\chi \approx 7$ after which a sudden drop in drag is noted for even younger windsea. The maximum in drag coefficient is connected to the assumption that surface gravity waves have a limiting steepness; for a wave age less than 10 the Phillips parameter is more or less constant and therefore the drag coefficient starts to decrease for decreasing wave age. For completeness, in the right panel of Fig. 6 the dependence of the different stress components of the

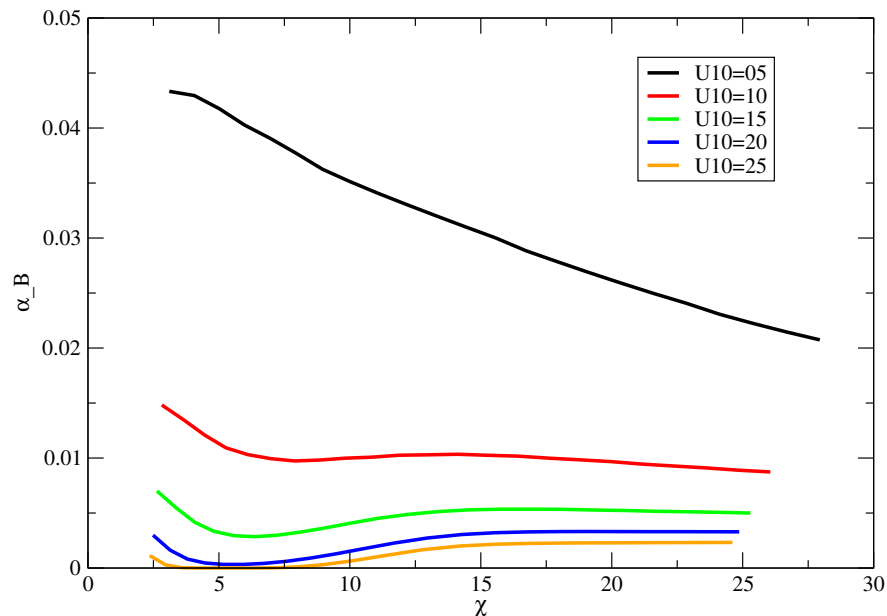


Figure 7: Comparison of dimensionless background roughness length gz_b/u_*^2 as function of wind age χ for different wind speeds.

momentum balance on wave age is also shown. For the relative high wind speed of 15 m/s the viscous stress plays a minor role in the stress balance at the surface. The low-frequency part of the wave-induced stress $\tau_{w,lf}/\tau_a$ always gives a substantial contribution to the total stress, but this is clearly not the case for its high-frequency part, which gives a small contribution in the wave age range from 3 to 11. The reason for the vanishing of the high-frequency stress is that the cut-off wavenumber k_c is below k_{3w} which is the starting point of the gravity-capillary wave spectrum. In other words, in that wave age range the stress is completely determined by the low-frequency stress, therefore, since in that range $\tau_a = \tau_{w,lf}$ it makes sense to compare the results from the iteration scheme with the simple expression for the low-

frequency wave-induced stress given by Eq. (46). Indeed, a comparison of the analytical result for the drag coefficient $C_D = \tau_w/U_{10}^2$ and the numerical result is shown in Fig. 6 and a good agreement is found for small wave ages where $\tau_a \approx \tau_{w,lf}$.

We are now in a position to determine the background roughness length, which is a quantity that originates from the theory of §2. Here, the unresolved stress $\tau_{w,hf}$ is represented by the turbulent stress τ_{turb} at the surface where the mixing length is given by $l(0) = \kappa z_b$. For the logarithmic profile (16) one then finds the simple relation

$$z_b = z_0 \sqrt{\tau_{w,hf}/\tau_a} \quad (57)$$

and in Fig. 7 the dimensionless background roughness length gz_b/u_*^2 is plotted as function of wave age for different wind speeds. In the present operational system the dimensionless background roughness length has the constant value of 0.0065 and only for the low wind speed of 10 m/s a fair agreement with the results of the explicit model for the background roughness is found. However, for higher wind speeds the reduction of wind wave growth at high frequencies is so large that a considerable dependence of the background roughness length on wave age is noted. As a consequence, the drag of airflow over really young wind waves is much less than anticipated from the present operational system. This has important consequences in particular for extreme conditions such as experienced in hurricane cases, as will be discussed in some more detail below. Finally, for winds speeds lower than 10 m/s the background roughness length is considerably larger than the operational choice of 0.0065, and, as a consequence the new formulation should have impact in particular in the Tropics where low wind speeds prevail.

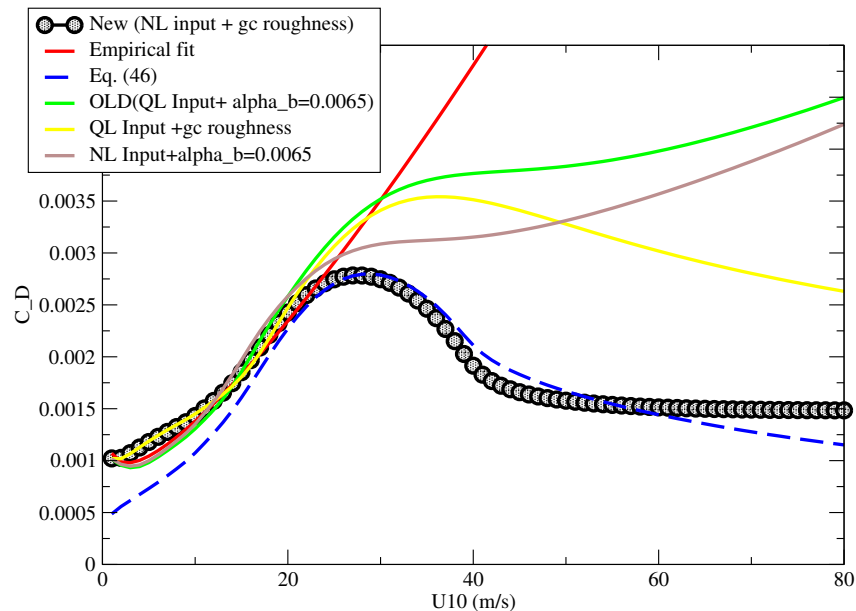


Figure 8: The climatological dependence of the drag coefficient C_D on wind speed U_{10} in the range of 1 to 80 m/s according to the old and the new approach. The analytical result (46) for the drag coefficient is shown for reference, while also Hersbachs climatological fit valid for low to moderate wind speeds is shown. In addition, the two final curves illustrate that the combination of Nonlinear input and the gravity-capillary background roughness is required to give a substantial reduction in drag for steep, high wind speed waves.

4.3 Climatology.

In order to conclude the discussion of the results of the coupled wind/wave system and the effects of the gravity-capillary waves and the nonlinear wind input it would be of interest to be able to study 'climatological' results for the drag coefficient so that a direct comparison with climatological results of the present ECMWF operational system can be made, as shown in the right panel of Fig. 3. However, presently we haven't introduced the new approach in the operational version of ecWAM and obtaining climatological results can be quite expensive, in particular when one is interested in extremes. Therefore, here we use a short-cut in order to obtain insight in the properties of the new approach. Using operational results obtained with the coupled IFS-ecWAM model one finds that on average there is a relation between wave age χ and wind speed U_{10} . In the wind speed range of $0 < U_{10} < 25$ it is approximately given by

$$\chi = \frac{35}{1 + 0.005U_{10}^2} \quad (58)$$

and it is assumed that the relation also holds for larger wind speed although we haven't been able to verify this because there were not sufficient extreme wind cases. Relation (58) expresses, in agreement with one's expectations, that the stage of development of the sea state generated by low wind speed event is much older than of extreme wind events.

The surface stress according to the present approach is now obtained using the JONSWAP spectrum with wave age given by Eq. (58) and the climatological relation between drag coefficient and wind speed is presented in Fig. 8. It is seen that for low wind speed, up to $U_{10} = 25$ m/s, the drag coefficient increases with wind speed in close agreement with a fit of mean drag coefficient versus wind speed found by Hersbach (cf. Edson *et al.* (2013)). This 'empirical' fit is only valid for wind speeds less than 23 m/s. For larger winds there are not enough reliable data yet (cf. Powell *et al.*, 2003; Jarosz *et al.*, 2007; Powell, 2008; Holthuijsen *et al.*, 2012), but these observations do suggest that the drag coefficient saturates and starts to decrease from $U_{10} = 30 - 35$ m/s onwards. The present model calculations seem to confirm this picture, in agreement with the analytical result (46).

Note that the analytical formula is valid for the case that the low-frequency wave-induced stress is dominant in the stress balance. This is indeed the case in the wind speed range 20-40 m/s as follows from Fig. 9, which shows the average Charnock parameter, the background Charnock parameter, and the viscous dimensionless length α_{visc} ⁵ as function of wind speed. Clearly the background roughness length becomes vanishingly small above a wind speed of around 20 m/s, hence the low-frequency wave-induced stress dominates the stress balance for larger wind speed up to 40 m/s.

Returning to Fig. 8 a comparison of the results of some sensitivity experiments is also shown. First, we show the climatological drag wind speed relation for the operational system which has a constant dimensionless background roughness length equal to 0.0065. These have the label OLD. In agreement with the actual operational results shown in the right panel of Fig. 3, the drag coefficient starts to saturate from a wind speed of about 30 m/s. But, clearly, there are significant differences between the operational results and the present approach. The main reason for this is that for large winds, when the waves become steep, the momentum transfer from the airflow to the high frequency waves is quenched, giving a considerable reduction of the background roughness and owing to the nonlinear wind input a considerable reduction of the low-frequency wave-induced stress. Furthermore, the last two experiments show that both the combination of a quasi-linear wind input and gravity-capillary roughness and the combination of nonlinear wind input and constant background roughness are not sufficient to have considerable reductions of drag at large wind. Clearly, this requires both a nonlinear wind input and a gravity-capillary roughness.

⁵ The viscous dimensionless length is defined as the viscous roughness length made dimensionless with the factor g/u_*^2 ,

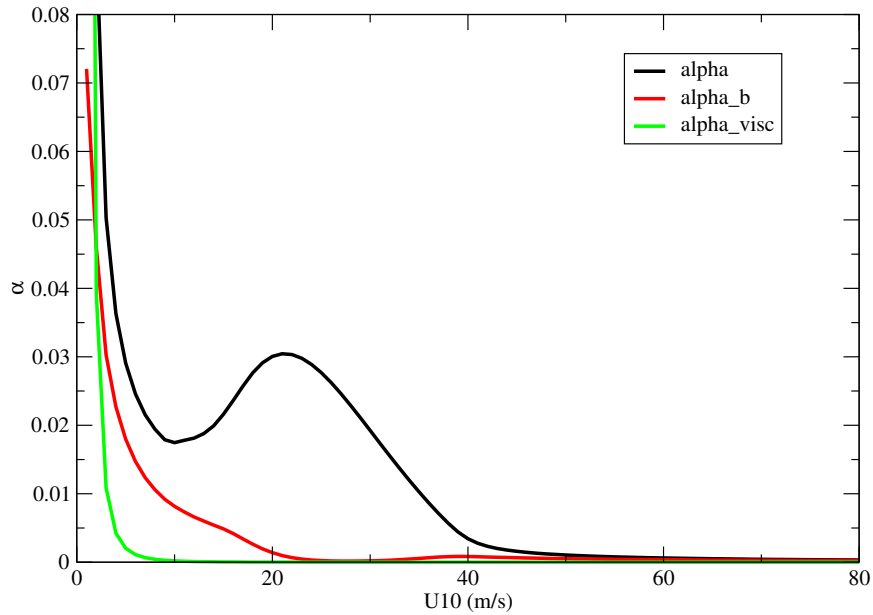


Figure 9: Climatological Charnock parameter α and background Charnock parameter α_b , as function of wind speed U_{10} .

Finally, it is also of interest to test the present wind-wave model for other aspects of the sea state as it could be a useful model for the interpretation of satellite remote sensing observations. For example, an Altimeter estimates the mean square slope (mss) of the sea surface, and hence it is of interest to see how well this model for the gravity waves and gravity-capillary waves is performing. In Fig. 10 a comparison for low wind speeds is made between the climatological mean square slope and observations from Cox and Munk (1954). It turns out that the mss is sensitive to a number of parameters in the VIERS model such as the starting wavenumber k_{3w} of the short wave spectrum and the strength of the three wave interactions α_3 . By choosing k_{3w} according to Eq. (50), with friction velocity dependent parameter γ , and by choosing $\alpha_3 = 6\pi$ a reasonable agreement with the Cox and Munk (1954) observations was achieved.

5 Towards an Operational implementation.

Thus far, we have developed a procedure to obtain the surface stress from the sum of stresses determined by the growth of long gravity waves, short gravity-capillary waves and by viscous effects. In this procedure the quasilinear wind input was replaced by the nonlinear wind input term given by (31) using the approximation (33). Now, briefly some aspects of the operational implementation of the present air-sea interaction procedure are discussed. Firstly, a fast approximate expression for the short wave spectrum is introduced and it is shown that the approximation gives accurate results for the drag coefficient and surface stress. In the next step this approach is implemented in a version of the ecWAM model and some of the initial results are discussed.

hence $\alpha_{visc} = g\bar{v}_a/u_*^3$, with $\bar{v}_a = 0.04v_a$.

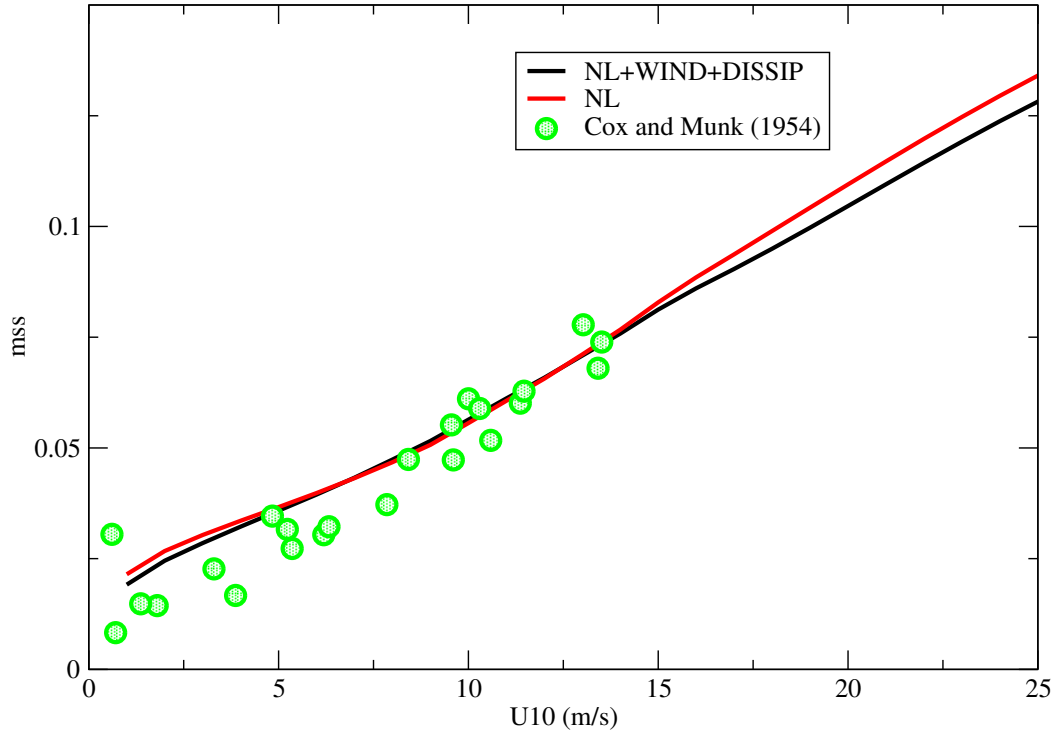


Figure 10: Comparison of modelled and observed mean square slope (mss) as function of wind speed. Also is shown impact on mss when inertial subrange spectrum is chosen.

5.1 Approximate short wave spectrum.

In order to speed up the calculations we have investigated the possibility to simplify the determination of the short wave spectrum. Inspecting the exact expression for the short wave spectrum as given in Eq. (54) it is clear there are two contributions, one from the nonlinear interactions giving the inertial subrange spectrum and one from input and dissipation. Usually it is thought that the inertial subrange spectrum is, compared to the contribution by input/dissipation, dominant. It is straightforward to test the assumption of the dominance of the inertial subrange spectrum by repeating the calculations of §4 for the drag coefficient but now with the contribution of input and dissipation to the short wave spectrum switched off. Hence, the degree of saturation spectrum is approximated by Eq. (55), i.e.

$$B \approx \left(\frac{\Phi_0}{2\alpha_3} \right)^{1/2} c_0^{-3/2} \frac{y(1+3y^2)^{1/2}}{(1+y^2)(y+y^3)^{1/4}}$$

where $y = k/k_0$, $k_0 = (g/T)^{1/2}$, $c_0 = (gT)^{1/4}$ and $\Phi_0 = \alpha_3 c^4 B_0^2 / \nu_g$ is the value of the energy flux at $k = k_{3w}$ which depends on the degree of saturation $B_0 = \alpha_p / 2$. Here, α_p is the Phillips parameter of the high-frequency part of the gravity wave spectrum. The starting wavenumber k_{3w} is given by Eq. (51).

The climatological results for the drag coefficient using the complete wave spectrum versus the inertial subrange spectrum have been compared in detail, and a very good agreement is found. In order to understand this better consider as a typical example a wind speed of 15 m/s. In Fig. 11 a comparison

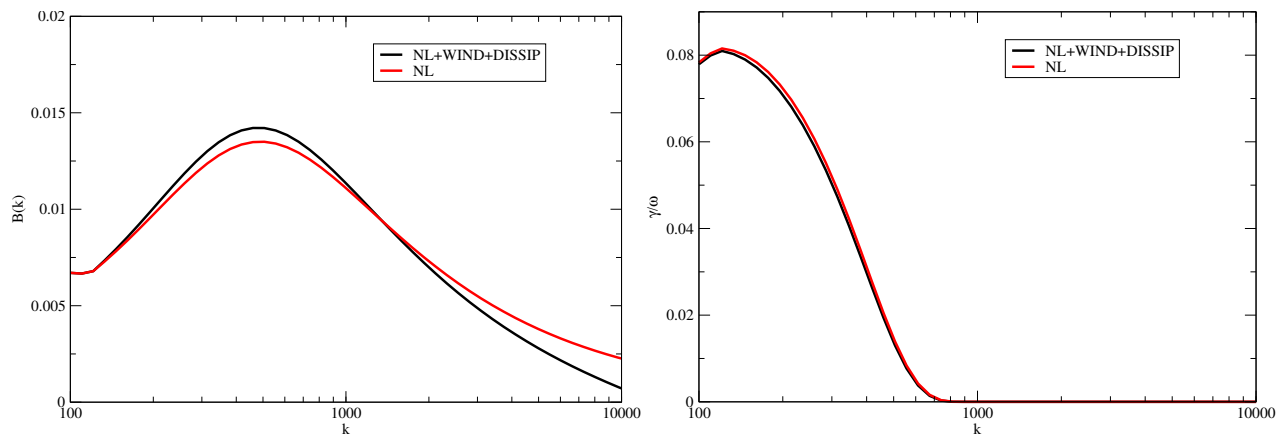


Figure 11: Left panel: comparison of degree of saturation spectrum using the full energy balance equation with the inertial sub range spectrum. The wind speed $U_{10} = 15$ m/s. Right panel shows the normalized wind input γ/ω as function of wavenumber for the same wind speed. Note the sharp fall-off in the region around wavenumber $k = 1000$ so that waves with a larger wavenumber do not contribute to the wave-induced stress.

between the wave spectrum based on the full energy balance equation and the inertial subrange spectrum is shown. Noting that the main interest is in an accurate representation of the wave-induced stress, in the right panel the growth rate of waves by wind is shown as well. Evidently, wind input vanishes for large wavenumber (in this case just k_c is just below 1000), so that the very short waves do not contribute to the wave-induced stress. Realizing this, it is clear that regarding the surface stress there is a very good agreement between inertial subrange spectrum and the complete spectrum.

It is concluded that for operational purposes it is a fair approximation to use the inertial subrange spectrum in the calculation of the wave-induced stress of the gravity-capillary waves. However, for the accuracy of mean square slope (mss) this may be a somewhat different matter because there is no high-wavenumber cut-off for this parameter. As shown in Fig. 10 for low wind speeds ($U_{10} < 20$ m/s) the inertial subrange spectrum gives an accurate mss but, although for larger wind speeds there are differences, these are believed to be relatively small.

5.2 Introduction into the ecWAM model.

In order to further test the present approach to determine the drag over sea waves we have implemented the new scheme into an older version of the ecWAM model, which is a single grid-point version of the wave physics introduced by Janssen (1991). This implementation was preceded by reprogramming the software regarding the determination of the high-frequency stress $\tau_{w,hf}$ and the stress τ_a in the surface layer. Previously, these quantities were determined by using tabulated values of $\tau_{w,hf}$ and τ_a at regular values of input parameters such as wind speed, Charnock parameter, etc. Reading from a table in memory is apparently relatively slow these days, and Bidlot (ECMWF, 2019) realized that one may as well do the actual calculation on the fly. So we upgraded the single-gridpoint version of the ecWAM software to allow for both iteration (for the surface stress) and the explicit calculation of $\tau_{w,hf}$ and τ_a and no slowing down of the running of the wave model was found. Having done this upgrade it was relatively straightforward to introduce the novel framework for calculation of the surface stress, including the actual

calculation of the surface roughness connected with the growth of gravity-capillary waves.

The upgraded ecWAM model, which used the nonlinear input term (31) with the exact renormalisation factors (32), has a number of parameters which need to be fixed. For the nonlinear transfer we are using DIA as implemented in ecWAM and have tuned the whitecap dissipation source term of CY45R1 with a dissipation coefficient $CDIS = 1.35$. The parameters for the wind input source function are $\beta_{max} = 1.3$, $z_{\alpha} = 0.008$ while the parameter α was renamed as α_b and was determined by the unresolved roughness calculation presented in this paper. Finally, the parameters of the numerical semi-implicit scheme were chosen as $XIMP = 2$ and $XDELFF = 5$.

In order to study the properties of the new wave modelling system a number of duration limited runs were made for wind speeds ranging from 1 to 25 m/s. The duration of the runs was one day. The first interesting parameter to study is the background roughness length $\alpha_b = gz_b/u_*^2$. In the previous model this parameter was assumed to be a constant and it is of interest to what extent this choice was a valid assumption. Results for α_b and the Charnock parameter α are shown for two wind speeds in Fig. 12.

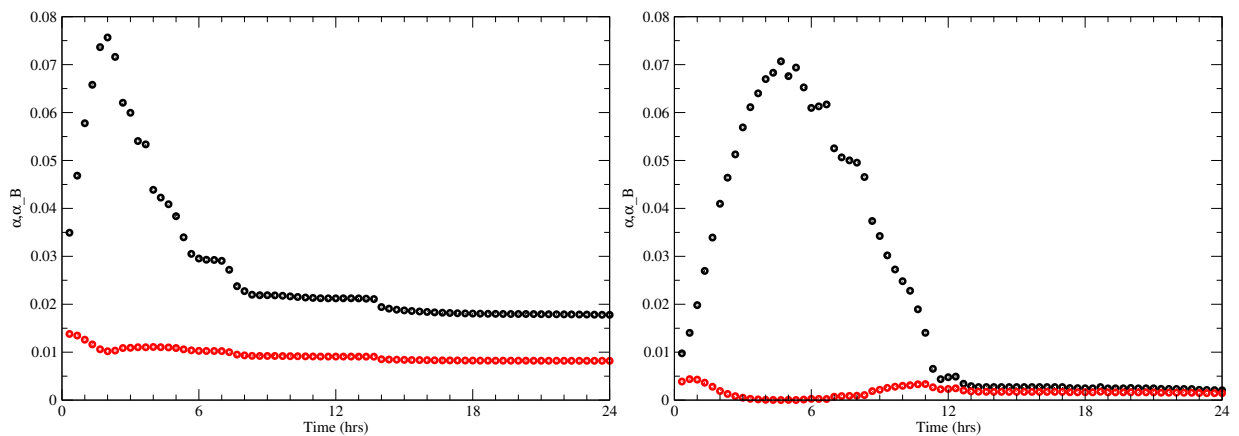


Figure 12: Evolution in time of Charnock parameter α (black circles) and background roughness α_b (red squares) for a wind speed of 10 m/s (left panel) and for a wind speed of 20 m/s (right panel).

Comparing this with Fig. 6 it is clear that there is a good agreement between the sophisticated wave model calculations of this Section and the simple model used in §4. Obviously, for typical wind speeds of the order of 10 m/s, the background roughness is fairly constant during the evolution of the sea state, thus for lower winds the assumption of a constant background roughness seems a valid one, although it should be pointed out that the smaller the wind speed the larger the background roughness α_b . In other words in low wind speed regions, e.g. in the deep Tropics, the new system will give rise to a larger surface drag. On the other hand, for strong winds and young windseas the background roughness is seen to vanish, resulting in a smoother water surface.

5.3 Breakdown of universality.

The discussion of results is concluded by noting that the introduction of the effects of gravity-capillary waves into the ecWAM model has caused a breakdown of the universality of the usual scaling relations

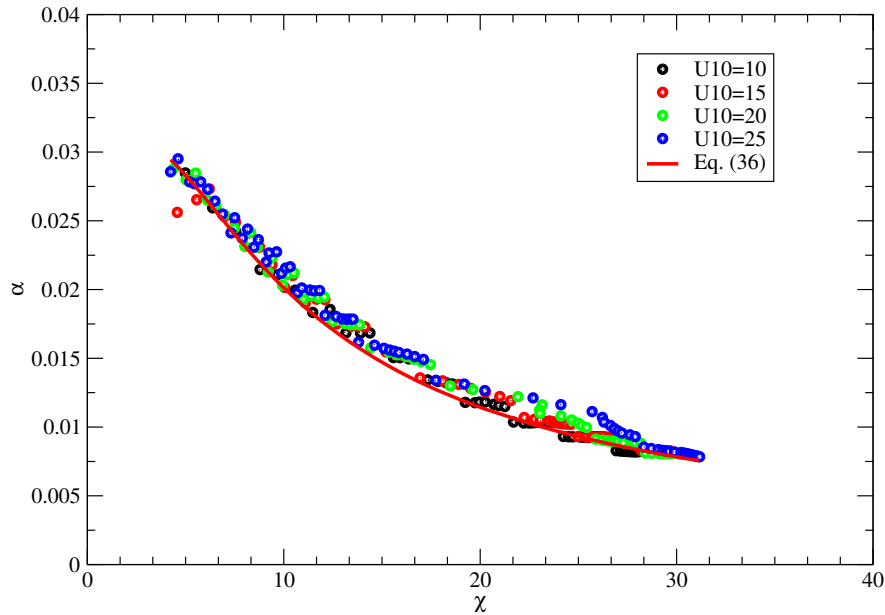


Figure 13: Dependence of Phillips parameter α_p on wave age $\chi = c_p/u_*$ for different wind speeds. The relation (36) is shown as well.

for wave growth, Charnock parameter, etc. Normally, it is possible to obtain universal scaling relations between parameters such as wave variance, peak period, wave age, etc. by scaling the relevant dimensional parameters by means of acceleration of gravity g and the friction velocity u_* , but for the present wave forecasting system this is not entirely feasible because the unresolved roughness depends on additional parameters such as surface tension, and air and water viscosity. In addition, it is noted that for low wind speed viscous damping has been introduced in the energy balance equation. However, one could still wonder to what extent universality holds.

As a first example, the dependence of the Phillips parameter α_p on the wave age parameter $\chi = c_p/u_*$ is studied. According to Eq. (36) a universal relation between these two parameters exists, and this relation is plotted in Fig. 13 together with the numerical results for α_p versus χ from the ecWAM model for wind speeds equal or larger than 10 m/s. Although the ecWAM model gives a small overestimate of the Phillips parameter, the agreement between numerical results and the parametrization (36) is good. Thus, it is fair to conclude that according to the new version of the ecWAM model the relation between Phillips parameter and wave age is universal. However, as will be seen in a moment this conclusion about universality does not hold for all parameters. An example is the relation between drag coefficient and wave age.

At the same time, one may wonder whether the discrepancy between modelled and observed Phillips parameter can be explained by a small underestimate of the surface stress, which may then give an overestimate of the wave age parameter, thus shifting the $\alpha_p - \chi$ relation towards larger values of χ . In order to check this, Fig. 14 gives a plot of drag coefficient at half the peak wavelength, $C_D(\lambda_p/2)$, as function of wave age for 4 different wind speeds and the numerical results are compared with Huang's parametrization (cf. Eq. (22)). Clearly, simulated drag coefficients are systematically somewhat lower than the ones according to Huang thus explaining why the simulated Phillips parameter in Fig. 13 is too

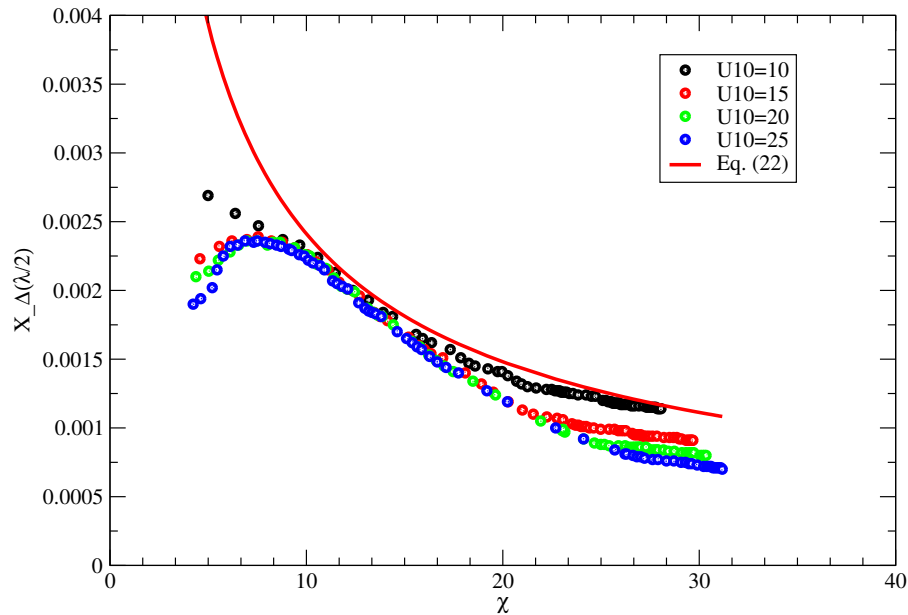


Figure 14: Comparison of modelled drag coefficient $C_D(\lambda/2)$ for different wind speeds with Huang’s empirical relation for the sea state dependent drag coefficient.

high compared to the parametrization (36). In addition, for wave ages larger than 15 agreement between numerical results and the Huang’s relation is lacking. At fixed waveage, for smaller winds $C_D(\lambda_p/2)$ is found to be systematically larger than for stronger winds. Near a waveage of 25 the relative difference amounts to 35%, but the strong winds (resp. 15, 20, 25 m/s) seem to cling together while the 10 m/s wind speed case is a relative outlier.

The above finding is confirmed by studying the dependence of the Charnock parameter α and the roughness associated with the gravity-capillary waves α_b on the wave age parameter. This is shown in Fig. 15 where in the left Panel numerical results for large wind speeds are shown and an approximate scaling behaviour is found. However, in the right Panel the cases of 10 and 15 m/s are compared and clearly the lower wind speed case deviates significantly from the higher wind speed case, again suggesting a break down in universality of the ‘classical’ scaling relations.

6 Conclusions.

In this paper we have discussed some new results on the generation of ocean waves by wind and the feedback of growing wind-waves on the airflow giving a strongly coupled air-water system. First of all, we have extended the wind input term which is based on Miles (1957) critical layer theory by including nonlinear effects which for strong winds give rise to a considerable reduction of the growth of surface gravity waves and of the associated wave-induced stress. This nonlinear effect is in particular important for strong winds, i.e. $U_{10} > 25 - 30$ m/s where, together with an explicit representation of the background roughness length, it will give rise to relatively small drag. It is emphasized that for moderate wind speeds the nonlinear effect on the wind input may be neglected.

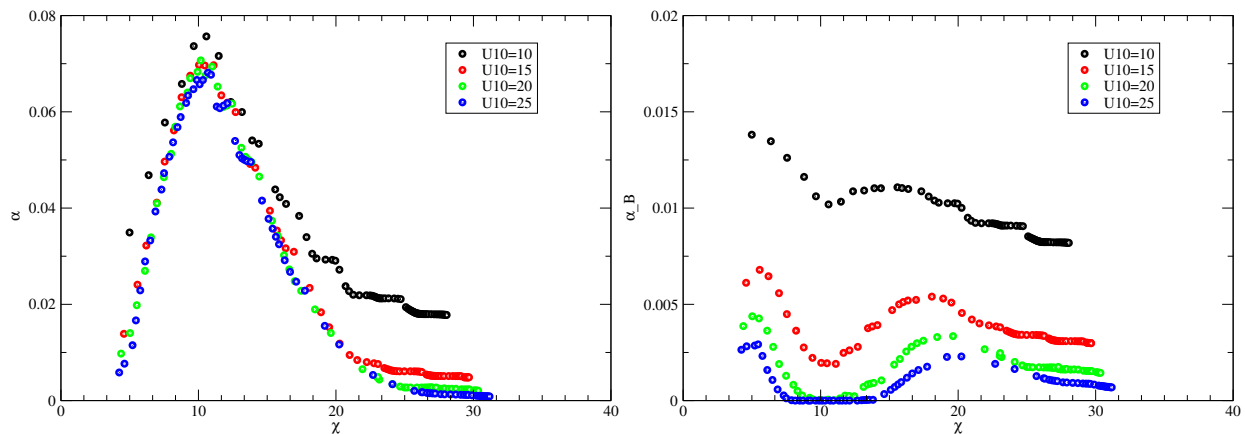


Figure 15: Charnock parameter α (left Panel) and background roughness α_b (right Panel) as function of wave age c_p/u_* . Deviations from friction velocity scaling are evident for old wind sea as the Charnock parameter is significantly larger for small wind speed.

Secondly, we have scrutinized the assumption of a constant dimensionless background roughness length. Originally, an explicit calculation of the slowing down of the airflow by surface gravity waves was made while the effect of the gravity-capillary waves was parametrized using a constant dimensionless background roughness length (see Eq. (2)). But this is a simplifying assumption which needs to be verified. For this reason we have introduced an explicit calculation of the amount of momentum gravity-capillary waves receive by using a model for the gravity-capillary waves which solves the one-dimensional energy balance equation for the short waves (the VIERS model). Again, the wind input is determined by a non-linear version of the critical layer theory of Miles (1957). As a consequence, for steep waves wind input to the short waves is quenched. In practice this means that when the sea state is nonlinear the gravity-capillary waves will hardly receive momentum from the wind so that the low-frequency wave-induced stress dominates the stress balance at the surface. Hence, the simple expression for the drag (see Eq. (46)) plays a prominent role in the air-sea interaction problem.

The consequences of this approach have been incorporated in a single gridpoint version of the ecWAM model. By relaxing the accuracy requirement (relative accuracy reduced from 0.001 % to 0.5 %) the solution of the surface stress balance only requires typically of the order of 5 iterations, thus making calculations of the surface stress on the fly practically feasible. The results from the new version of the ecWAM model are consistent with the simple model presented in §3. For example for large winds the background roughness is small for young wind waves. As a consequence, it is emphasized that for young windsea the classical scaling relations for e.g. wave variance, peak frequency and Phillips parameter still hold but for old wind sea this is not the case anymore, because for old windsea the background roughness is finite and depends on additional parameters such as the surface tension, and viscosity in air and water.

Appendices.

A Introducing three dimensional effects.

A.1 Basic Equations.

We follow the treatment of two-dimensional problem in Janssen (2004) and extend it to three dimensions. Our starting point is the set of equations for an adiabatic fluid with an infinite sound speed. Hence

$$\begin{aligned}\nabla \cdot \mathbf{u} &= 0, \\ \frac{d}{dt} \mathbf{u} &= -\frac{1}{\rho} \nabla p + \mathbf{g}, \\ \frac{d}{dt} \rho &= 0,\end{aligned}\tag{A1}$$

where all symbols have their usual meaning. We would like to study the stability of the equilibrium solution Eq. (A1) which corresponds to a flat air-sea interface. The equilibrium of interest is

$$\mathbf{u}_0 = U_0(z) \mathbf{e}_x, \quad \mathbf{g} = -g \mathbf{e}_z,$$

$$\rho_0 = \rho(z), \quad p_0(z) = -g \int dz \rho_0(z),\tag{A2}$$

where \mathbf{e}_x and \mathbf{e}_z are unit vectors in the x - and z -direction. Thus, we deal with a plane parallel flow whose speed and density only depend on height z . The equations for an adiabatic fluid do not explain the height dependence of wind speed and density because effects of small-scale turbulence are not taken into account. In addition, effects of turbulence on the wave-induced motion in the air are not considered.

In order to test the stability of the equilibrium (A2) one linearizes around the equilibrium, assuming that the perturbations are small and one takes normal modes of the form

$$\mathbf{u} = \hat{\mathbf{u}} \exp i(k_x x + k_y y - \omega t),\tag{A3}$$

with k_x and k_y the wavenumbers in the x and y direction while ω is the unknown angular frequency. Here, for given wavenumbers k_x and k_y the task is to obtain ω from the boundary value problem for the vertical velocity or displacement. Dropping the hats, this boundary value problem follows from the linearized equations

$$ik_x u + ik_y v + w' = 0,\tag{A4}$$

$$ik_x W u + w W' = -\frac{ik_x}{\rho_0} p_1,\tag{A5}$$

$$ik_x W v = -\frac{ik_y}{\rho_0} p_1,\tag{A6}$$

$$ik_x W w = \rho_1 \frac{p_0'}{\rho_0^2} - \frac{p_1'}{\rho_0},\tag{A7}$$

$$ik_x W \rho_1 + w \rho_0' = 0,\tag{A8}$$

where $W = U_0 - c_x$ and $c_x = \omega/k_x$ is the x -component of the phase speed of the surface gravity wave. Introducing the perturbation of the streamlines $\psi = w/W$ one obtains after some algebra the following

differential equation for ψ

$$\frac{d}{dz} \left(\rho_0 W^2 \frac{d}{dz} \psi \right) = \left[(k_x^2 + k_y^2) \rho_0 W^2 + \frac{k_x^2 + k_y^2}{k_x^2} g \rho_0' \right] \psi. \quad (\text{A9})$$

A special point in this equation is the location $z = z_c$ (with z_c called the critical height) where the Doppler shifted velocity W vanishes:

$$W = U_0 - c_x = 0, \quad U_0 = \frac{u_*}{\kappa} \log\left(1 + \frac{z_c}{z_0}\right) = c_x$$

hence

$$z_c = z_0 \left[\exp\left(\frac{\kappa c_x}{u_*}\right) - 1 \right]. \quad (\text{A10})$$

In order to simplify things introduce polar coordinates

$$k_x = k \cos \theta, \quad k_y = k \sin \theta, \quad (\text{A11})$$

so that the Doppler shifted velocity becomes $W = U_0 - c / \cos \theta$ with $c = \omega / k$ (k is the total wavenumber) and

$$z_c = z_0 \left[\exp\left(\frac{\kappa c}{u_* \cos \theta}\right) - 1 \right]. \quad (\text{A12})$$

and the differential equation for ψ becomes

$$\frac{d}{dz} \left(\rho_0 W^2 \frac{d}{dz} \psi \right) = (k^2 \rho_0 W^2 + \tilde{g} \rho_0') \psi. \quad (\text{A13})$$

with $\tilde{g} = g / \cos^2 \theta$. This equation has the same form as the problem in 2D, but with g replaced by \tilde{g} while c in W is replaced by $c / \cos \theta$. Therefore results for the 2 D problem can immediately be used to write down the solution for the 3D problem.

Remark: There is an alternative way to proceed. Multiply (A13) by $\cos^2 \theta$, then the differential equation becomes

$$\frac{d}{dz} \left(\rho_0 W^2 \frac{d}{dz} \psi \right) = (k^2 \rho_0 W^2 + g \rho_0') \psi.$$

where now $W = U_0 \cos \theta - c$. This is elegant because when waves propagate under an angle θ with the wind, this form of the problem immediately shows that these waves will experience the effective wind $U_0 \cos \theta$.

A.2 Growth rate in 3D.

In order to determine the growthrate of the waves one needs to solve the boundary value problem consisting of the differential equation (A13) and the boundary condition of vanishing ψ at $|z| \rightarrow \infty$.

In Janssen (2004) the boundary value problem for the 2-D case has been solved for the case of a jump in the density profile, representing wind blowing over a water surface at $z = 0$. The 3D solution now follows immediately by replacing the celerity c by $c / \cos \theta$ and acceleration of gravity g by $g / \cos^2 \theta$. In 2D the solution reads

$$c^2 = \frac{g(1 - \varepsilon)}{k - \varepsilon \psi_a'(0)}, \quad (\text{A14})$$

with $\varepsilon = \rho_a/\rho_w$ is the air-water density ratio, while ψ follows from the solution of the boundary value problem in air, i.e.

$$\begin{aligned} \frac{d}{dz} \left(W^2 \frac{d}{dz} \psi_a \right) &= k^2 W^2 \psi_a, \\ \psi_a(0) &= 1, \quad \psi_a \rightarrow 0 \text{ for } z \rightarrow \infty, \end{aligned} \quad (\text{A15})$$

because a constant density in air was assumed. Remarkably, after replacing c and g in Eq. (A14) to obtain the 3D answer, it turns out that the form of the expression for the complex phase speed in 2D and 3D is identical, but the solution for the streamline perturbation will be different because it depends through W on $\cos \theta$.

The problem (A14)-(A15) can be solved in an approximate manner since $\varepsilon \ll 1$. Using now the vertical component of the wave-induced velocity in stead of the displacement of the streamlines $\psi = w/W$ one finds from (A13) in terms of the normalised velocity $\chi = w/w(0)$ the Rayleigh equation

$$\begin{aligned} W_0 \left(\frac{d^2}{dz^2} - k^2 \right) \chi &= W_0'' \chi, \\ \chi(0) &= 1, \quad \chi \rightarrow 0 \text{ for } z \rightarrow \infty, \end{aligned} \quad (\text{A16})$$

where $W_0 = U_0 - c_0$ and $c_0 = \sqrt{g/k}$. The growth rate γ_E of the energy of the waves then follows from solving Eq. (A14) to first order in ε . As a result

$$\frac{\gamma_E}{\varepsilon \omega_0} = \frac{1}{2k} \mathcal{W}(\chi, \chi^*)|_{z=0}, \quad (\text{A17})$$

where the Wronskian is given by $\mathcal{W} = -i(\chi' \chi^* - \chi'^* \chi)$. This is Miles classical result in disguise. This follows from Janssen (2004) who has shown that

$$\mathcal{W} = -2\pi \frac{W_{0c}''}{|W_{0c}'|} |\chi_c|^2, \text{ for } z < z_c.$$

Therefore, there is wave growth if the curvature of the wind profile is negative (Miles, 1957) while in two dimensions, for large times, owing to the feedback of the waves on the windprofile, the curvature in the wind profile vanishes (Janssen, 1982).

For a logarithmic wind profile

$$U_0 = \frac{u_*}{\kappa} \log(1 + z/z_0) \quad (\text{A18})$$

the problem can be solved in an approximate manner (see e.g. Miles, 1993). This approximate solution is only valid for slow waves. Janssen (2004) adopted Miles approximate solution but changed the coefficients so that also an accurate solution for fast waves was obtained. One finds

$$\frac{\gamma_E}{\omega_0} = \varepsilon \beta \left(\frac{u_*}{c} \right)^2 \quad (\text{A19})$$

with

$$\beta = \frac{1.2}{\kappa^2} y_c \log^4(y_c), \quad y_c \leq 1, \quad y_c = kz_c \quad (\text{A20})$$

where

$$y_c = kz_0 e^{\kappa/x}, \quad x = u_*/c + z_\alpha, \quad z_\alpha = 0.08. \quad (\text{A21})$$

after some adjustment of parameters.

The three dimensional answer now follows immediately by replacing c by $c/\cos\theta$ and g by $g/\cos^2\theta$. As a result one finds

$$\frac{\gamma E}{\omega_0} = \varepsilon \beta \left(\frac{u_*}{c}\right)^2 \cos^2 \theta \quad (\text{A22})$$

where β is given by (A20) and y_c involves a $\cos\theta$ factor as well

$$y_c = kz_0 e^{\kappa/x}, \quad x = (u_*/c + z_\alpha) \cos \theta. \quad (\text{A23})$$

A.3 Wave-induced stress in 3D.

The principle goal of this section is to determine the wave-induced stress in terms of the vertical velocity profile. Note that in 3D the wave-induced stress has two components, one along the wind direction and one across. The along and cross components are connected on the one hand to wind-wave growth and on the other hand to stretching of the vortex. First, the stress for a single wave is obtained and then this is followed by an expression for many waves that are characterized by the wave spectrum.

The wave stress along the wind, with wind pointing in the x -direction, is given by

$$\tau_w^{(x)} = -\langle uw \rangle.$$

Writing for fluctuating components of the velocity

$$\mathbf{u} = \hat{\mathbf{u}} e^{i\theta} + c.c.,$$

where the phase is given by $\theta = k_x x + k_y y - \omega t$, and dropping the hats, the x -component of the wave stress becomes

$$\tau_w^x = -uw^* + c.c. \quad (\text{A24})$$

Hence, we require u in terms of w . From (A4) we find u in terms of v and w . Now v can be expressed in terms of u and w by using (A5) and (A6). This gives

$$v = \frac{k_y}{k_x} u - \frac{ik_y}{k_x^2} \frac{W'_0}{W_0} w. \quad (\text{A25})$$

Substitution of (A25) in (A4) then gives

$$u = \frac{ik_y^2}{k_x(k_x^2 + k_y^2)} \frac{W'_0}{W_0} w + \frac{ik_x}{k_x^2 + k_y^2} w', \quad (\text{A26})$$

and note that for one-dimensional propagation one finds the familiar relation $u = iw'/k_x$ as k_y vanishes. Then, using (A24), the wave-induced stress in the x -direction becomes

$$\tau_w^{(x)} = \frac{-ik_y^2}{k_x(k_x^2 + k_y^2)} \frac{W'_0}{W_0} |w|^2 + \frac{-ik_x}{k_x^2 + k_y^2} w^* w' + c.c. \quad (\text{A27})$$

In the next step we connect this to the surface elevation η through $\partial\eta/\partial t = w$ at $z = 0$. Write $w = w_0\chi$ where χ satisfies the Rayleigh equation with boundary condition $\chi(0) = 1$. One finds $-i\omega\eta = w_0$, hence

$$w = -i\omega\eta\chi.$$

Using this, and introducing polar coordinates Eq. (A27) becomes

$$\tau_w^{(x)} = \frac{\omega^2 \sin^2 \theta}{k \cos \theta} |\eta|^2 |\chi|^2 \left(\frac{i}{W_0^*} - \frac{i}{W_0} \right) \frac{\partial}{\partial z} U_0 + \frac{\omega^2}{k} \cos \theta |\eta|^2 \mathscr{W}(\chi, \chi^*). \quad (\text{A28})$$

where \mathscr{W} is the Wronskian of the Rayleigh equation, introduced below Eq. (A17). For growing waves one has

$$\frac{1}{W_0} = \frac{P}{W_0} + \pi i \delta(W_0),$$

and after some rearrangement one obtains for the wave-induced stress

$$\tau_w^{(x)} = \frac{\omega^2}{k} \cos \theta |\eta|^2 \left[2\pi \tan^2 \theta |\chi|^2 \delta(W_0) \frac{\partial}{\partial z} U_0 + \mathscr{W}(\chi, \chi^*) \right]. \quad (\text{A29})$$

The first term is new. It is connected with vortex stretching (v-component of the velocity) and gives rise to diffusion of momentum. The second term is the one that occurs also for one-dimensional propagation and this term will give rise to diffusion of vorticity.

In the case of many waves we write for the surface elevation

$$\eta = \int d\mathbf{k} \hat{\eta} e^{i\mathbf{k}\cdot\mathbf{x}} + c.c. \quad (\text{A30})$$

and we use the closure relation

$$\langle \eta_1 \eta_2^* \rangle = \frac{1}{2} F(\mathbf{k}_1) \delta(\mathbf{k}_1 - \mathbf{k}_2). \quad (\text{A31})$$

where $F(\mathbf{k})$ is the wavenumber spectrum. After some algebra the x -component of the wave-induced stress becomes

$$\tau_w^{(x)} = D_\perp \frac{\partial}{\partial z} U_0 + \frac{1}{2} \int d\mathbf{k} \frac{\omega^2}{k} \cos \theta F(k, \theta) \mathscr{W}(\chi, \chi^*) \quad (\text{A32})$$

with

$$D_\perp = 2\pi \int d\theta \omega k^2 F(k, \theta) \sin^2 \theta |\chi|^2.$$

Given the stress in (A32) one can now work out the rate of change of the wind velocity, i.e.

$$\frac{\partial}{\partial t} U_0 = \frac{\partial}{\partial z} \tau_w^{(x)} = \frac{\partial}{\partial z} D_\perp \frac{\partial}{\partial z} U_0 + \frac{1}{2} \int d\mathbf{k} \frac{\omega^2}{k} \cos \theta F(k, \theta) \frac{\partial}{\partial z} \mathscr{W}(\chi, \chi^*) \quad (\text{A33})$$

Now the first derivative of the Wronskian \mathscr{W} may be eliminated using the Rayleigh equation and as a result one obtains

$$\frac{\partial}{\partial t} U_0 = \frac{\partial}{\partial z} D_\perp \frac{\partial}{\partial z} U_0 + D_\parallel \frac{\partial^2}{\partial z^2} U_0 \quad (\text{A34})$$

with

$$D_\parallel = \pi \int d\mathbf{k} \frac{\omega^2}{k} \cos \theta F(k, \theta) |\chi|^2 \delta(W_0) \quad (\text{A35})$$

where $W_0 = U_0 - c/\cos\theta$. Evaluating the integral over k and using the linear dispersion relation for surface gravity waves so that $v_g = c/2$, the parallel diffusion coefficient has, apart from the θ -dependence, a very similar form as the perpendicular diffusion coefficient, hence

$$(D_{\parallel}, D_{\perp}) = 2\pi \int_{|\theta| \leq \pi/2} d\theta \omega k^2 F(k, \theta) (\cos^2 \theta, \sin^2 \theta) |\chi|^2. \quad (\text{A36})$$

Note that in the above expression the wavenumber k is expressed in terms of the vertical coordinate z through the resonance condition $W_0 = U_0 - c/\cos\theta = 0$ where here the phase speed follows from the dispersion relation of free gravity waves. The resonance condition also implies a restriction for the integration in the θ domain: only those waves are included that have a (positive) projection onto the wind direction, i.e. $|\theta| \leq \pi/2$.

In a similar fashion one may evaluate the cross stress

$$\tau_w^{(y)} = -\langle vw \rangle \quad (\text{A37})$$

For a single wave one obtains

$$\tau_w^{(y)} = \frac{\omega^2}{k} \sin\theta |\eta|^2 [-2\pi |\chi|^2 W_0' \delta(W_0) + \mathscr{W}(\chi, \chi^*)] \quad (\text{A38})$$

Following the same procedure as on the previous pages one may obtain the wave-induced stress for a spectrum of gravity waves, i.e.

$$\tau_w^{(y)} = -D_c \frac{\partial}{\partial z} U_0 + \frac{1}{2} \int dk d\theta \omega^2 \sin\theta F(k, \theta) \mathscr{W}(\chi, \chi^*) \quad (\text{A39})$$

where

$$D_c = 2\pi \int_{|\theta| \leq \pi/2} d\theta \omega k^2 |\chi|^2 F(k, \theta) \sin\theta \cos\theta. \quad (\text{A40})$$

The rate of change in time of the y -component of the mean velocity then becomes

$$\frac{\partial}{\partial t} V = -\frac{\partial}{\partial z} D_c \frac{\partial}{\partial z} U_0 + D_c \frac{\partial^2}{\partial z^2} U_0. \quad (\text{A41})$$

and remarkably the diffusion coefficients of the two processes are the same.

This derivation assumes that the wind speed is in the x -direction, but clearly this leads to a contradiction in case there is a finite cross diffusion coefficient D_c , caused by an asymmetrical distribution of surface gravity waves around the wind direction, because finite D_c will according to Eq. (A41) generate a finite wind speed in the y -direction. In the main part of the paper we will make the assumption that the cross diffusion coefficient vanishes so that no appreciable y -component of the wind is generated. This is a reasonable assumption since most of the stress is determined by the short waves that are very quickly in equilibrium with the wind.

Nevertheless, it is of interest to see what happens when the restriction of having only an x -component of the mean flow is abandoned. Therefore, let us assume that now the equilibrium flow has both an x - and a y -component so that $\mathbf{u}_0 = U_0(z, t)\mathbf{e}_x + V_0(z, t)\mathbf{e}_y$. We will not give the details of the calculations, because they are similar to the ones already presented, but only the main result is given, i.e. the mean flow equations in the presence of gravity waves become

$$\frac{\partial}{\partial t} U_0 = \frac{\partial}{\partial z} D_{\perp} \frac{\partial}{\partial z} U_0 + D_{\parallel} \frac{\partial^2}{\partial z^2} U_0 - \frac{\partial}{\partial z} D_c \frac{\partial}{\partial z} V_0 + D_c \frac{\partial^2}{\partial z^2} V_0, \quad (\text{A42})$$

while the equation for the y -component of the velocity is obtained by swapping U_0 and V_0 in the above equation, hence

$$\frac{\partial}{\partial t} V_0 = \frac{\partial}{\partial z} D_{\perp} \frac{\partial}{\partial z} V_0 + D_{\parallel} \frac{\partial^2}{\partial z^2} V_0 - \frac{\partial}{\partial z} D_c \frac{\partial}{\partial z} U_0 + D_c \frac{\partial^2}{\partial z^2} U_0. \quad (\text{A43})$$

It would be of interest to study the consequences of this set of coupled equations for the evolution of wind waves and surface winds, but so far this has not been done.

References.

- Ardhuin, F., Rogers, E., Babanin, A.V., Filipot, J.F., Magne, R., Roland, A., *et al.* (2010). Semiempirical Dissipation Source Functions for Ocean Waves. Part I: Definition, Calibration, and Validation. *J. Phys. Oceanogr.* **40**, 1917-1941. doi: 10.1175/2010jpo4324.1.
- Caudal, G., 2002. A physical model for the narrowing of the directional sea wave spectra in the short gravity to gravity-capillary range. *J. Geophys. Research* **107**(C10),3148, doi:10.1029/2000JC000437.
- Cox, C.S. and W.H. Munk, 1954. Statistics of the sea surface derived from sun glitter. *J. Marine Res.* **13**, 198-227.
- Donelan, M.A., 1982. The dependence of the aerodynamic drag coefficient on wave parameters, p381-387 in: Proc. of the first international conference on meteorological and air/sea interaction of the coastal zone; Amer. Meteor. Soc., Boston, Mass.
- Donelan, M.A., 2018, On the decrease of the oceanic drag coefficient in high winds. *J. Geophys. Research: Oceans*, **123**,1485-1501. <https://doi.org/10.1002/2017JC013394>
- Donelan, M.A. and W.J. Plant, 2009. A threshold for wind-wave growth. *J. Geophys. Research* **114**,C07012. <https://doi.org/10.1029/2008JC005238>
- Driest, E.R. van, 1951. Turbulent boundary layer in compressible fluids. *J. Aero. Sci.* **18**, 145-160.
- ECMWF, 2019: IFS Documentation CY46R1. Tech. rep., ECMWF.
- ECMWF, 2020: IFS Documentation CY47R1. Tech. rep., ECMWF.
- Edson J.B., V. Jampana, R.A. Weller, S.P. Bigorre, A.J. Pluedemann, C.W. Fairall, S.D. Miller, L. Mahrt, D. Vickers and H. Hersbach, 2013. On the exchange of Momentum over the Open Ocean, *J. Phys. Oceanogr.* **43**, 1378-1391.
- Fabrikant, A.L., 1976. Quasilinear theory of wind-wave generation. *Izv. Atmos. Ocean. Phys.* **12**, 524-526.
- Günther, H., 1981. A parametric surface wave model and the statistics of the prediction parameters. PhD thesis, Univ. Hamburg, 90p.
- Hasselmann, K., T.P. Barnett, E. Bouws, H. Carlson, D.E. Cartwright, K. Enke, J.A. Ewing, H. Gienapp, D.E. Hasselmann, P. Kruseman, A. Meerburg, P. Müller, D.J. Olbers, K. Richter, W. Sell and H. Walden, 1973. Measurements of wind-wave growth and swell decay during the Joint North Sea Wave Project (JONSWAP), *Dtsch. Hydrogr. Z. Suppl. A* **8**(12), 95p.
- Holthuijsen, L.H., M.D. Powell, and J.D. Pietrzak, 2012. Wind and waves in extreme hurricanes. *J. Geophys. Research* **117**(C09003). <https://doi.org/10.1029/2012JC007983>.

- Huang P.A., 2005. Temporal and spatial variation of the drag coefficient of a developing sea under steady wind-forcing. *J. Geophys. Res.* **110**, C07024. doi:10.1029/2005JC002912
- Jähne, B., and K.S. Riemer, 1990. Two-dimensional wavenumber spectra of small-scale water surface waves, *J. Geophys. Res.* **95**, 11,531-11,546.
- Janssen, J.A.M., and H. Wallbrink, 1997. SATVIEW: a semi-physical scatterometer algorithm, KNMI Scientific Report WR 97-03.
- Janssen, P.A.E.M., 1982. Quasilinear approximation for the spectrum of wind-generated water waves. *J. Fluid Mech.* **117**, 493-506.
- Janssen P.A.E.M., 1989. Wave-induced stress and the drag of air flow over sea waves, *J. Phys. Oceanogr.* **19** 745-754.
- Janssen P.A.E.M., 1991. Quasi-linear theory of wind wave generation applied to wave forecasting. *J. Phys. Oceanogr.* **21**, 1631-1642.
- Janssen, P.A.E.M., 1992. Experimental evidence of the effect of surface waves on the airflow. *J. Phys. Oceanogr.* **22**, 1600-1604.
- Janssen, P., 2004. *The interaction of Ocean Waves and Wind*. Cambridge University Press, 300+viii pp.
- Janssen, P.A.E.M., H. Wallbrink, C.J. Calkoen, D. van Halsema, W.A. Oost and P. Snoeij, 1998. VIERS-1 scatterometer model. *J. Geophys. Research* **103**, 7807-7831.
- Jarosz, E., D.A. Mitchell, D.W. Wang, and W.J. Teague, 2007. Bottom-up determination of air-sea exchange under a major tropical cyclone. *Science*, **315**(5819),1707-1709.
- Kitaigorodskii, S.A., 1962. Application of the theory of similarity to the analysis of wind-generated water waves as a stochastic process, *Bull. Acad. Sci. USSR Geophys. Ser. no. 1*, 73p.
- Kudryavtsev, V.N. and V.K. Makin, 2007. Aerodynamic roughness of the sea surface at high winds. *Boundary Layer Meteorol.* **125**, 289-303.
- Kitaigorodskii, S.A., 1983. On the theory of the equilibrium range in the spectrum of wind-generated gravity waves. *J. Phys. Oceanogr.* **13**, 816-827.
- Kukulka, T., Hara, T. and S.E. Belcher, 2007. A model of the air-sea momentum flux and breaking-wave distribution for strongly forced wind waves. *J. Phys. Oceanogr.* **37**, 1811-1828.
- Magnusson, L., Bidlot, J.R., Bonavita, M., Brown, A., Browne, P., De Chiara, G., Dahoui, M., Lang, S. T. K., McNally, T., Mogensen, K. S., Pappenberger, F., Prates, F., Rabier, F., Richardson, D. S., and Vitart, F. (2019). ECMWF activities for improved hurricane forecasts. *Bulletin of the American Meteorological Society*, 100, 445458. <https://doi.org/10.1175/BAMS180044.1>
- Makin, V.K. (2005). A note on drag of the sea surface at hurricane winds. *Boundary Layer Meteorol.*, **115**, 169-176.
- Miles, J.W., 1957. On the generation of surface waves by shear flows. *J. Fluid Mech.* **3**, 185-204.
- Miles, J.W., 1965. A note on the interaction between surface waves and wind profiles. *J. Fluid Mech.* **22**, 823-827.
- Miles, J.W., 1993. Surface wave generation revisited. *J. Fluid Mech.* **256**, 427-441.
- Phillips, O.M., 1985. Spectral and statistical properties of the equilibrium range in wind-generated

gravity waves. *J. Fluid Mech.* **156**, 505-531.

Plant, W.J., 1982. A relation between wind stress and wave slope. *J. Geophys. Res.* **C87**, 1961-1967.

Powell, M.D., P.J. Vickery, and T.A. Reinhold, 2003. Reduced drag coefficient for high wind speeds in tropical cyclones. *Nature* **422**(6929), 279-283.

Powell, M.D., 2008. New findings on hurricane intensity, wind field extent and surface drag coefficient behavior. *Proceedings of the tenth international workshop on wave hindcasting and forecasting and coastal hazard symposium*, North Shore, Oahu, Hawaii, 11-16 November 2007.

Smith S.D., R.J. Anderson, W.A. Oost, C. Kraan, N. Maat, J. DeCosmo, K.B. Katsaros, K.L. Davidson, K. Bumke, L. Hasse and H.M. Chadwick, 1992. Sea surface wind stress and drag coefficients: the HEXOS results. *Boundary Layer Meteorol.* **60**, 109-142.

Troitskaya, Y.L., Sergeev, D.A., Kandaurov, A.A., Baidakov, G.A., Vdovin, M.A. and V.I. Kazakov, 2012. Laboratory and theoretical modeling of air-sea momentum transfer under severe wind conditions. *J. Geophys. Res.* **117**, C00J21.